Quaternary Science Reviews xxx (xxxx) xxx

Contents lists available at ScienceDirect

Quaternary Science Reviews

journal homepage: www.elsevier.com/locate/quascirev

Southern Ocean link between changes in atmospheric CO_2 levels and northern-hemisphere climate anomalies during the last two glacial periods

Julia Gottschalk [a, b, c, *], Luke C. Skinner [a], Samuel L. Jaccard [b], Laurie Menviel [d], Christoph Nehrbass-Ahles [a, e], Claire Waelbroeck [f]

[a] Godwin Laboratory for Palaeoclimate Research, Department of Earth Sciences, University of Cambridge, Cambridge, UK
[b] Institute of Geological Sciences and Oeschger Centre for Climate Change Research, University of Bern, Bern, Switzerland
[c] Lamont-Doherty Earth Observatory, Columbia University, Palisades, NY, USA
[d] Climate Change Research Centre, PANGEA, University of New South Wales, Sydney, New South Wales, Australia
[e] Climate and Environmental Physics, Physics Institute, Oeschger Centre for Climate Change Research, University of Bern, Bern, Switzerland
[f] Laboratoire des Sciences du Climat et de l'Environnement, LSCE/IPSL, CNRS-CEA-UVSQ, Université de Paris-Saclay, Gif-sur-Yvette, France

ARTICLE INFO

Article history:
Received 21 January 2019
Received in revised form
8 November 2019
Accepted 10 November 2019
Available online xxx

Keywords:
Glacials
Palaeoclimatology
Southern Ocean
Redox-sensitive elements
Carbon cycle
Foraminifera
Dansgaard-Oeschger cycles
Atmospheric CO_2 variations
Stadials
Interstadials

ABSTRACT

Past millennial-scale changes in atmospheric CO_2 ($CO_{2,atm}$) concentrations have often been attributed to variations in the overturning timescale of the ocean that result in changes in the marine carbon inventory. Yet, there remains a paucity of proxy evidence that documents changes in marine carbon storage globally, and that links them to abrupt climate variability in the northern hemisphere associated with perturbations of the Atlantic Meridional Overturning Circulation (AMOC). The last two glacial periods were suggested to differ in the spatial extent of the AMOC and its sensitivity to perturbations. This provides an opportunity to compare the nature of marine carbon cycle-climate feedbacks between them. Here, we reconstruct variations in respired carbon storage (via oxygenation) and the AMOC "geometry" (via carbonate ion saturation) in the deep South Atlantic. We infer decreases in deep South Atlantic respired carbon levels at times of weakened AMOC and rising $CO_{2,atm}$ concentrations during both glacial periods. These findings suggest a consistent pattern of increased Southern Ocean convection and/or air-sea CO_2 fluxes during northern-hemisphere stadials accompanying AMOC perturbations and promoting a rise in $CO_{2,atm}$ levels. We find that net ocean carbon loss, and hence the magnitude of $CO_{2,atm}$ rise, is largely determined by the stadial duration. North Atlantic climate anomalies therefore affect Southern Ocean carbon cycling in a consistent manner, through oceanic (e.g., ventilation seesaw) and/or atmospheric processes (e.g., Ekman pumping).

1. Introduction

Changes in the concentration of CO_2 in the atmosphere ($CO_{2,atm}$) recorded in Antarctic ice cores have been found to be tightly linked with Antarctic temperature proxies over the past eight glacial cycles (e.g., Fischer et al., 2010). This link can be partly explained by the radiative forcing imparted by $CO_{2,atm}$ (i.e., the greenhouse effect; e.g., Köhler et al., 2017), and by the temperature dependence of processes governing global ocean- and land-atmosphere CO_2 exchange, such as the ocean CO_2 solubility (Bacastow, 1996), metabolic rates of plants and phytoplankton (Eppley, 1972; Policy et al., 1993; Matsumoto, 2007) and organic carbon respiration rates in the ocean (Matsumoto, 2007; Matsumoto et al., 2007; Kwon et al., 2009). However, this link is also thought to rely on a variety of biogeochemical and hydrographic feedback mechanisms that affect the deep- and surface ocean's total carbon- and alkalinity levels (e.g., Sigman and Boyle, 2000; Hain et al., 2010; Cartapanis et al., 2018). The ocean's sizeable carbon reservoir exchanges with the atmosphere on centennial- to millennial timescales, in particular through vertical mixing and Ekman pumping in the Southern Ocean (Primeau, 2005; Marinov et al., 2006; Gebbie and Huybers, 2011). Other potential carbon sources/sinks that

* Corresponding author. Lamont-Doherty Earth Observatory, Columbia University, Palisades, NY, USA.
E-mail address: jgottsch@ldeo.columbia.edu (J. Gottschalk).

https://doi.org/10.1016/j.quascirev.2019.106067
0277-3791/

may have influenced $CO_{2,atm}$ concentrations on these timescales include the terrestrial biosphere (Köhler et al., 2005; Menviel et al., 2008; Bozbiyik et al., 2011), Arctic permafrost (Zech, 2012; Köhler et al., 2014; Tesi et al., 2016) and the mantle/lithosphere (Huybers and Langmuir, 2009; Broecker et al., 2015; Lund et al., 2016). The Southern Ocean bears a strong leverage on the efficiency of ocean-atmosphere gas exchange (i.e., the "ocean CO_2 solubility pump") and on the global-ocean pre-formed versus respired nutrient ratio (i.e., the "soft-tissue/organic carbon pump"), while also influencing global-ocean alkalinity (i.e., the "hard-tissue/carbonate pump"). The Southern Ocean is therefore assumed to have played a dominant role in past $CO_{2,atm}$ changes (Sarmiento and Toggweiler, 1984; Volk and Hoffert, 1985; Broecker et al., 1999; Sigman and Boyle, 2000; Ito and Follows, 2005; Fischer et al., 2010; Hain et al., 2010; Sigman et al., 2010).

Proxy evidence from the Southern Ocean covering the last glacial cycle strongly supports this view. The glacial Antarctic Zone of the Southern Ocean, south of the glacial Polar Front (Fig. 1), has provided proxy evidence for reduced vertical mixing and stronger water column density stratification during peak glacial periods, suggesting increased carbon sequestration from the atmosphere (e.g., François et al., 1997; Skinner et al., 2010; Jaccard et al., 2013; Roberts et al., 2015; Studer et al., 2015). In addition, an extended seasonal Antarctic sea ice zone during these intervals may have curbed air-sea gas exchange (Stephens and Keeling, 2000; Gersonde et al., 2003; Benz et al., 2016), acting to further decrease $CO_{2,atm}$. In the glacial sub-Antarctic Zone between the sub-Antarctic and sub-Tropical Front (Fig. 1), enhanced supply of aeolian dust that may have alleviated iron-limitation imposed on phytoplankton growth (Martin, 1990; Shoenfelt et al., 2018) is thought to have led to increased carbon export and $CO_{2,atm}$ drawdown during the last peak glacial (Kumar et al., 1995; Ziegler et al., 2013; Anderson et al., 2014; Lamy et al., 2014; Martínez-García et al., 2014; Gottschalk et al., 2016a; Jaccard et al., 2016). These biological and hydrographic conditions were suggested to have relaxed over the last deglaciation and during Antarctic warming intervals, reducing the biological export of carbon to the deep ocean, and exposing the deep-ocean carbon reservoir to the atmosphere through enhanced vertical mixing and air-sea gas exchange in the Southern Ocean, causing a rise of $CO_{2,atm}$ (e.g., Anderson et al., 2009; Skinner et al., 2010, 2014; Gottschalk et al., 2016a; Jaccard et al., 2016; Ronge et al., 2016; Sikes et al., 2016; Basak et al., 2018; Rae et al., 2018). In addition, these processes are thought to be closely connected to North Atlantic climate and parallel perturbations in the Atlantic Meridional Overturning Circulation (AMOC) (Sigman et al., 2007; Anderson and Carr, 2010; Charles et al., 2010; Denton et al., 2010; Lee et al., 2011; Chiang et al., 2018). Specifically, CO_2 evasion from the Southern Ocean may have been promoted through a poleward shift and/or intensifications of the southern-hemisphere westerlies (SHW) and an associated increase in Ekman pumping (Toggweiler et al., 2006; Anderson et al., 2009; Denton et al., 2010; Lee et al., 2011), surface buoyancy variations in the Southern Ocean (Watson and Naveira Garabato, 2006; Watson et al., 2015), Antarctic sea ice retreat and/or the rejuvenation of Southern Ocean deep waters (i.e., a "bipolar ventilation seesaw"; Skinner et al., 2010, 2014). These scenarios highlight separate atmospheric and oceanic pathways (though not mutually exclusive), by which northern-hemisphere climate variability might affect the respired carbon budgets and marine carbon cycling in the Southern Ocean (Buizert et al., 2018). Their relative contributions to $CO_{2,atm}$ change remain, however, unclear.

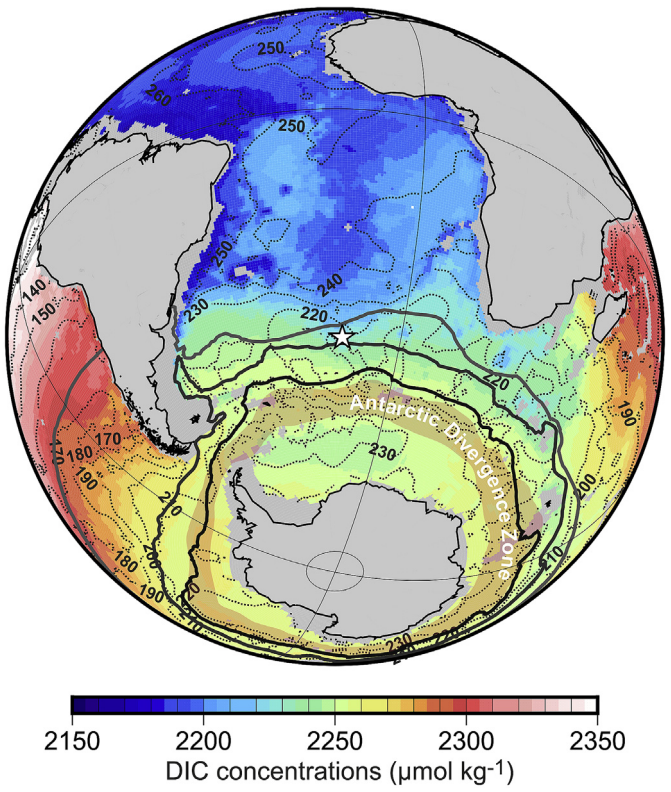

Fig. 1. Location of the study site. Concentration of dissolved inorganic carbon (DIC, shaded; Key et al., 2004) in the ocean averaged below 2.5 km water depth. Contours indicate the average seawater dissolved [O_2] below 2.5 km water depth (Garcia et al., 2014). The location of sediment cores MD07-3076Q and MD07-3077 is indicated by a star. Major fronts are shown as stippled lines from south to north: Polar Front (dark grey line), sub-Antarctic Front (grey line) and sub-Tropical Front (light grey line) (Orsi et al., 1995; Sokolov and Rintoul, 2009). The Antarctic Divergence Zone is highlighted by an orange circumpolar band, representing the region of strong positive air-sea CO_2 fluxes in austral winter in the Southern Ocean at present-day (see maps in Takahashi et al., 2002).

An important test of the classical view of a primary role of Southern Ocean processes in driving millennial-scale $CO_{2,atm}$ variations and their connection to North Atlantic climate anomalies gained from proxy records of the last 70 kyr can be made by extending the analyses to older millennial-scale climate events. The penultimate glacial period, i.e., Marine Isotope Stage (MIS) 6, may prove particularly useful for this undertaking, because MIS 6 was characterised by slightly different climatic conditions compared to the last glacial period (i.e., MIS 3), in particular with respect to the extent of northern-hemisphere ice sheets (Svendsen et al., 2004) and the strength of the hydrological cycle (Margari et al., 2010). These differences have likely led to a weaker AMOC during MIS 6 that may be associated with lower-amplitude changes in Antarctic temperature (Margari et al., 2010). We hypothesise that the sensitivity of the ocean carbon system to perturbations was likely different during both glacial periods, and a comparison between the two may therefore provide important insights into the dependency of respired carbon changes in the deep South Atlantic and $CO_{2,atm}$ variations to the nature, timing and duration of North Atlantic climate events and overall glacial conditions.

Here, we assess and compare changes in respired carbon content in the Atlantic sector of the Southern Ocean and the AMOC geometry during the last two glacial periods based on sub-Antarctic Atlantic sediment cores MD07-3076Q (14.20°W, 44.10°S, 3777 m water depth) and MD07-3077 (14.23°W, 44.15°S, 3776 m water depth). Respired carbon changes are derived from qualitative and quantitative estimates of bottom water oxygen concentrations ([O_2]), which are reflected in the enrichment of redox-sensitive elements in foraminiferal authigenic coatings (Gottschalk et al.,

Please cite this article as: Gottschalk, J et al., Southern Ocean link between changes in atmospheric CO_2 levels and northern-hemisphere climate anomalies during the last two glacial periods, Quaternary Science Reviews, https://doi.org/10.1016/j.quascirev.2019.106067

2016a) and epibenthic-to-deep infaunal foraminiferal $\delta^{13}C$ gradients (Hoogakker et al., 2015). Reconstructions of AMOC changes are based on partial sedimentary dissolution proxies that track variations in bottom water carbonate ion saturation. These proxies are sensitive to the presence of northern-sourced (carbonate oversaturated) and southern-sourced (carbonate undersaturated) water masses, as well as water mass end-member changes, at our study site (Gottschalk et al., 2015a). Additional analyses of past changes in local productivity approximated by determinations of the sedimentary opal content (e.g., Anderson et al., 2014) and cryosphere dynamics based on the abundance of ice-rafted debris (IRD; e.g., Kanfoush et al., 2000; Nielsen et al., 2007) help to assess the roles of ocea biology and sea ice/icebergs in Southern Ocean carbon cycle dynamics, respectively.

2. Study area

Sediment cores MD07-3076Q and MD07-3077 were retrieved from the eastern flank of the Mid-Atlantic Ocean Ridge and are located within the sub-Antarctic Zone of the Atlantic sector of the Southern Ocean (Fig. 1). The cores were collected at the same site using different coring techniques, i.e., by square kasten- and piston coring, respectively. With a length of 10.9 m, MD07-3076Q covers the last ~100 kyr, while its sister core MD07-3077 has a length of 49.5 m and extends back to 450 kyr before present (BP) (Vázquez Riveiros et al., 2010). Analyses for MIS 3 were performed in core MD07-3076Q, while those for MIS 6 are based on MD07-3077.

The core sites are currently bathed in Lower Circumpolar Deep Water (LCDW), which is a mixture of DIC-rich and low-$[CO_3^{2-}]$ Antarctic Bottom Water (AABW), derivatives of DIC-rich and low-$[CO_3^{2-}]$ Indian and Pacific Deep Water and DIC-low and high-$[CO_3^{2-}]$ North Atlantic Deep Water (NADW) (Carter et al., 2009; Talley, 2013). Our site is characterised by slight carbonate (i.e., calcite) oversaturation ($\Omega = [CO_3^{2-}]_{in-situ}/[CO_3^{2-}]_{saturated} = 1.09$), but is proximal to carbonate-undersaturated water masses located deeper in the South Atlantic water column. It is therefore sensitive to changes in the preponderance of high-$[CO_3^{2-}]$ NADW and low-$[CO_3^{2-}]$ AABW in the deep South Atlantic through associated changes in carbonate saturation at the core site (Gottschalk et al., 2015a). The modern $[O_2]$ at our core site is 215 μmol kg^{-1} (Garcia et al., 2014).

3. Methods

3.1. Respired carbon levels

Respired carbon levels are directly linked to apparent oxygenation utilization (AOU) in the ocean, which reflects the drawdown of O_2 due to the respiration of organic matter (Kroopnick, 1985; Jaccard et al., 2014; Galbraith and Jaccard, 2015). AOU changes were suggested to be the main driver of deep-ocean $[O_2]$ changes, because saturation $[O_2]$ in the ocean varied little over glacial-interglacial timescales (Jaccard and Galbraith, 2012; Galbraith and Jaccard, 2015). We therefore reconstruct bottom water $[O_2]$ to assess respired carbon changes during the last two glacial periods using the following two independent approaches in order to circumvent potential limitations and biases that may come with the analysis of a single proxy.

3.1.1. Uranium enrichment in foraminiferal coatings

The enrichment of uranium (U) in marine sediments is mainly a result of reducing conditions in pore waters of marine sub-surficial sediments (Anderson et al., 1989; Barnes and Cochran, 1990; Klinkhammer and Palmer, 1991; Morford and Emerson, 1999; McManus et al., 2006; Tribovillard et al., 2006). Most of the soluble uranyl (U^{VI}) carbonate ions that are reduced to insoluble uraninite (U^{IV} or U^{III}) under oxygen-depleted conditions in pore waters diffuse from the water column into the sediment (Barnes and Cochran, 1990; Klinkhammer and Palmer, 1991; Morford and Emerson, 1999; Zheng et al., 2002). Uraninite precipitates on any substrate within marine sediments, including detrital material and carbonate shells of foraminiferal tests, resulting in a co-variation of authigenic U levels of bulk sediments and foraminiferal coatings (Boiteau et al., 2012; Chen et al., 2017).

Owing to the very low U concentrations within the carbonate lattice of foraminiferal shells (<~20 nmol mol^{-1}) (Russell et al., 2004; Yu and Elderfield, 2007; Yu et al., 2008; Raitzsch et al., 2011) compared to those measured on non-reductively cleaned bulk (carbonate lattice and authigenic coating) foraminiferal shells (up to 700 nmol mol^{-1}) (Boiteau et al., 2012; Gottschalk et al., 2016a; Lear et al., 2016), the U/Ca ratio of bulk foraminifera obtained by inductively coupled plasma-mass spectrometry (ICP-MS) are dominated by U/Ca ratios of authigenic coatings. As the thickness of the shells and the size of the foraminifera may have varied over time (Barker and Elderfield, 2002) and may have had an impact on foraminiferal U/Ca ratios, it was suggested that normalization to manganese (Mn) might alleviate morphological biases (Gottschalk et al., 2016a). Under oxic conditions, Mn^{II} is oxidised and precipitates as insoluble Mn^{IV} or Mn^{III} oxyhydroxides (Calvert and Pedersen, 1996). Under reducing conditions, these Mn oxides dissolve releasing Mn^{II} that may be precipitated as Mn-carbonates below the anoxic boundary, or diffuse upward to the oxic zone, where it can be recycled (Froelich et al., 1979; Tribovillard et al., 2006). As foraminiferal tests in marine sediments act as a nucleus for the accumulation of both solid U- and Mn-phases, these phases are found to accumulate in coatings inside and/or outside of the foraminiferal shell (Pena et al., 2005, 2008; Hasenfratz et al., 2016; Detlef et al., 2020). Foraminiferal U/Mn ratios, along with U/Ca ratios (Boiteau et al., 2012), were hence suggested to be sensitive to and indicative of changes in bottom water oxygenation (Gottschalk et al., 2016a; Chen et al., 2017; Detlef et al., 2020).

However, Chen et al. (2017) do not find a close relationship between core-top epibenthic foraminiferal U/Mn ratios and bottom water $[O_2]$. This may not be surprising, because the redox-cycling of U was suggested to be closely linked to that of Fe (Barnes and Cochran, 1990; Zheng et al., 2002), and hence occurs a few centimeters below the sediment-water interface, and may thus not be recorded by core-top foraminifera. This becomes evident in the tandem analyses of planktonic foraminiferal coatings and pore-waters in multi-cores from a well-oxygenated setting performed by Skinner et al. (2019), which show that foraminiferal Mn/Ca ratios track the pore-water Mn^{2+} concentration (with enrichment of both below the anoxic boundary), while foraminiferal U/Ca ratios track the loss of dissolved U from pore-waters through precipitation of U-compounds in oxygen-depleted sub-surface sediments (slightly lower than the zone of Mn accumulation). These findings emphasise a separation of early diagenetic reactions involving U and Mn in sub-surface sediments (Froelich et al., 1979). This is consistent with recent work by Detlef et al., 2020, who observe a *correlation* of foraminiferal U/Ca and Mn/Ca ratios in Bering Sea sediments, suggesting the accumulation of Mn in authigenic or recrystallised carbonate phases in foraminiferal coatings, possibly under anoxic conditions. The authors suggest that the increase in U accumulation over Mn accumulation in foraminiferal coatings in this setting is proportional to diagenetic alteration, and hence possibly dependent on bottom water $[O_2]$ conditions. In contrast, Boiteau et al. (2012) show an *anticorrelation* of foraminiferal U/Ca and Mn/Ca in foraminiferal samples from the Southeast Atlantic, emphasising

Please cite this article as: Gottschalk, J et al., Southern Ocean link between changes in atmospheric CO_2 levels and northern-hemisphere climate anomalies during the last two glacial periods, Quaternary Science Reviews, https://doi.org/10.1016/j.quascirev.2019.106067

different oxic and anoxic pathways of diagenetic precipitation of solid U- and Mn-phases. Further investigation is needed to fully understand the mechanisms driving the U/Mn proxy. Nonetheless, despite the different processes driving U- and Mn precipitation on foraminiferal shell, there is a strong connection to redox-chemical cycling in sub-marine sediments that is in turn tightly coupled to the availability of oxygen in bottom waters (Boiteau et al., 2012; Gottschalk et al., 2016a; Chen et al., 2017; Detlef et al., 2020; Skinner et al., 2019). In our study, we analyse the U enrichment in authigenic coatings on several foraminiferal species, and report the associated U/Ca and U/Mn ratios.

The foraminiferal record of redox-sensitive elements may be influenced by post-depositional deepening of the anoxic boundary, which may cause authigenic U compounds to be oxidised and redissolved ("burned-down") (Zheng et al., 2002; Kasten et al., 2003; McManus et al., 2005). As we find high sedimentation rates of 10–15 cm kyr^{-1} during MIS 3 and 6, we assume that the observed U/Ca and U/Mn ratios represent signals that mostly formed in equilibrium with bottom waters, with little overprints from non-steady state processes. We argue that the temporal offset between our redox-sensitive proxy changes and contemporaneous shifts in other foraminiferal proxies during past glacials is limited to a maximum of 0.5–1 kyr, assuming maximum oxygen penetration depths into sub-surface sediments of ~5–7 cm during past glacials. This is supported by a good agreement of foraminiferal U/Ca and U/Mn ratios with other bottom water oxygenation proxies and ventilation age changes over the last glacial cycle at the core site (Gottschalk et al., 2016a; Skinner et al., 2019).

U/Ca- and U/Mn analyses were performed on the planktonic foraminifer *Globigerina bulloides* (20–30 specimens; 250–300 μm size fraction) and *Globorotalia inflata* (20–30 specimens; >212 μm size fraction) for MIS 6 and Termination (T) II, and on *G. bulloides* (20–30 specimens; 250–300 μm size fraction) and the benthic foraminifer *Uvigerina* spp. (5–15 specimens; 250–300 μm size fraction) for MIS 3 and TI. Prior to ICP-MS analyses, the foraminiferal samples were cleaned through clay removal and silicate picking (Barker et al., 2003; Boiteau et al., 2012). The reproducibility of U/Ca and U/Mn ratios of replicate samples is within 30 nmol mol^{-1} and 0.08 mmol mol^{-1} (1σ, $n = 6$), respectively.

3.1.2. Epibenthic-deep infaunal foraminiferal $\delta^{13}C$ gradients

The benthic foraminifer *Globobulimina affinis* is thought to actively migrate towards the low-oxygen microhabitat near or at the anoxic boundary within marine sub-surface sediments (Geslin et al., 2004), and has therefore a deep infaunal habitat (Corliss and Emerson, 1990; McCorkle et al., 1990). The $\delta^{13}C$ offset of *G. affinis* from bottom water (i.e., from the supposedly epibenthic foraminifer *Cibicidoides kullenbergi*), $\Delta\delta^{13}C_{Ck\text{-}Ga}$, has been proposed to record the depletion of pore water $\delta^{13}C$ due to organic carbon respiration. This is thought to be controlled by bottom water oxygen diffusion into the sediment that is a function of bottom water [O_2] itself (McCorkle and Emerson, 1988; McCorkle et al., 1990; Hoogakker et al., 2015). We use the $\Delta\delta^{13}C$–bottom water [O_2] calibration of Hoogakker et al. (2015) to obtain quantitative estimates of bottom water [O_2] at our core sites during the past two glacial periods.

We have performed stable isotopic analyses on *G. affinis* and *C. kullenbergi* on one to four specimens of the >150 μm size fraction. The analysed *C. kullenbergi* specimens refer to the *sensu lato*-morphotype as illustrated in Gottschalk et al. (2016b). The samples were measured on Finnigan Δ+ and Elementar Isoprime mass spectrometers at the LSCE in Gif-sur-Yvette (France). Prior to the analyses, foraminifera were rinsed with methanol, ultrasonicated for 10 s, dried at room temperature, and finally roasted under vacuum at ~380 °C for 45 min to remove contaminant organic phases or detritus.

The oxygen and carbon isotopic shell composition is expressed as $\delta^{18}O$ and $\delta^{13}C$ in ‰ versus Vienna Pee Dee Belemnite (VPDB). VPDB is defined with respect to the National Bureau of Standards (NBS)-19 calcite standard ($\delta^{18}O = -2.20$‰ and $\delta^{13}C = +1.95$‰) (Coplen, 1988). The mean external reproducibility of our carbonate standards is $\sigma = 0.05$‰ ($\delta^{18}O$) and $\sigma = 0.03$‰ ($\delta^{13}C$), and the measured NBS-18 $\delta^{18}O$ and $\delta^{13}C$ values are -23.2 ± 0.2‰ VPDB and -5.0 ± 0.1‰ VPDB, respectively.

3.2. Deep South Atlantic carbonate ion saturation as an indicator of the Atlantic overturning geometry

Partial sedimentary dissolution proxies, such as the benthic-to-planktonic (Be/Pl) foraminiferal ratio, planktonic foraminifer abundances or the planktonic foraminiferal fragmentation, are sensitive to the carbonate saturation (i.e., corrosiveness) of deep South Atlantic bottom waters in our study area (Barker and Diz, 2014; Gottschalk et al., 2015a, 2018). We have normalised and averaged these three proxy records from our study site for each glacial period in order to obtain the 'carbonate saturation index' (Gottschalk et al., 2015a). This index qualitatively reflects the southward advance of high-[CO_3^{2-}] NADW (Gottschalk et al., 2015a). However, given the complex processes affecting this proxy (such as changes in water mass end-members, local sedimentation rate and sediment porosity), it does not represent changes in the strength of the AMOC in a quantitative way.

Be/Pl ratios, planktonic foraminifer abundances and the foraminifer fragmentation were determined by sedimentary census counts of a sample aliquot of the >150 μm-fraction (CLIMAP project members, 1984). At least 300 planktonic foraminifera were counted for each sample, which also allowed an estimation of sea surface temperature (SST) changes at the core site based on planktonic foraminiferal assemblages and the Southern Ocean calibration of Haddam et al. (2016). The abundance of planktonic foraminifera is expressed as number per gram dry bulk sediment (>150 μm), while the fragmentation represents the percent fraction of planktonic foraminifer fragments (when larger than half a broken shell) of the total abundance of planktonic foraminifera and fragments. The reproducibility of reported planktonic foraminifer abundances, planktonic foraminifer fragmentation and the Be/Pl ratio has been inferred from 15 duplicate counts, and is within 6000 g^{-1}, 1.9% and 0.014 (1σ), respectively.

3.3. Opal as an indicator for export production

The sedimentary biogenic silica (opal) content in our study cores was quantified by Fourier Transform Infrared Spectroscopy (FTIRS; Vogel et al., 2016) using a Vertex 70 FTIR-spectrometer (Bruker Optics Inc.). Repeating the analyses of parts of the record in MIS 3 and MIS 6 indicate the robustness of relative changes in sedimentary opal. However, absolute values may differ from wet-chemical opal analyses by 2.6 ± 2.6% ($n = 112$) during MIS 3 (Gottschalk et al., 2016a) and by 4.5 ± 1.6% ($n = 55$) across different FTIRS sample batches during MIS 6 (Supplementary Fig. S1). This may be associated with a bias of FTIR spectra due to a small residual water content in the samples (Vogel et al., 2016) that we were not able to eliminate despite several precautionary measures. Because absorbed water in the samples biases the opal content towards higher values, we have corrected all individual datasets onto those opal records with the lowest absolute values (based on calculated offsets

Please cite this article as: Gottschalk, J et al., Southern Ocean link between changes in atmospheric CO_2 levels and northern-hemisphere climate anomalies during the last two glacial periods, Quaternary Science Reviews, https://doi.org/10.1016/j.quascirev.2019.106067

in overlapping sections, Supplementary Fig. S1).

3.4. Ice-rafted detritus as an indicator of sea ice and/or iceberg export

The abundance of IRD was assessed alongside the census counts of fragmented shells and foraminifera (see section 3.2.). It is reported as percentage with respect to the total number of sediment grains (including foraminifera and fragments). The reproducibility of estimated IRD percentages is within 1.5% (1σ, $n = 15$).

3.5. Chronology

Chronological control of sediment core MD07-3076Q younger than 27 kyr BP is based on calibrated radiocarbon ages of monospecific planktonic foraminifera samples, which have been adjusted for variations in surface ocean reservoir ages (Skinner et al., 2010). The age models of cores MD07-3076Q (i.e., for MIS 3) and MD07-3077 (i.e., for MIS 6) are based on a stratigraphic alignment of abundance peaks of *G. bulloides* with maxima in Antarctic air-temperature, represented by peaks in the EPICA (European Project for Ice Coring in Antarctica) Dome C (EDC) δD Antarctic ice-core record (Jouzel et al., 2007) (Fig. 2). This approach assumes that temperature-sensitive *G. bulloides* abundance variations at our South Atlantic core site and Antarctic air-temperatures (at EDC) co-vary. We therefore take the age model for >27 kyr BP for our core site from a previous study that used this approach (Channell et al., 2017) with minor revision of three tiepoints during MIS 6 (encircled symbols in Fig. 2a), in order to produce a better match of *G. bulloides* variations with Antarctic air-temperature (The depths of two of these tiepoints (174.6 and 177.4 kyr) were shifted 20 cm towards the top of the core, and the tiepoint at ~2490 cm was shifted by 1 kyr towards older ages). Our simple approach is consistent with another age model approach that has been applied to study millennial-scale variability at our core site based on the first time derivative of EDC δD, as demonstrated in Gottschalk et al., 2015a. During TII, we use the age control points of Gottschalk et al., 2016b that are based on an alignment of abundance variations of *Neogloboquadrina pachyderma* with EDC δD. Although this age model approach may deviate from an age model based on *G. bulloides* abundance variations (cf. Fig. 2), these age uncertainties are not relevant for the objectives of this paper.

Resulting sedimentation rates range between 5 cm kyr^{-1} during the last deglaciation and 15 cm kyr^{-1} during MIS 3 and MIS 6 (Fig. 2). We apply a 700 yr ad-hoc error for each of our planktonic abundance-based tiepoints (not considering absolute age uncertainties of the EDC chronology of up to 2.4 kyr in MIS 3 and 3 kyr in MIS 6), which translates into a relative age uncertainty of 1.7 ± 0.5 kyr during MIS 3 and 1.8 ± 0.8 kyr during MIS 6 and TII with respect to the Antarctic AICC2012 ice age scale (Bazin et al., 2013; Veres et al., 2013). These age uncertainties were estimated based on Monte Carlo simulations with the Bayesian software package Bchron (Haslett and Parnell, 2008), and consider potential sedimentation rate changes in between our selected tiepoints. Although the millennial-scale accuracy of our age model is limited, circumstantial support for our age model alignment comes from benthic (*Cibicidoides* sp.) $\delta^{18}O$ analyses. During both MIS 3 and MIS 6, we observe a good agreement on millennial timescales between the benthic $\delta^{18}O$ records at our sub-Antarctic Atlantic site and sediment core MD01-2444 from the Iberian margin in the North Atlantic (2.6 km water depth, Fig. 2; Skinner et al., 2007; Margari et al., 2010), although both records are on entirely independent agescales. Benthic $\delta^{18}O$ records are not per se expected to co-vary in the Atlantic (given the finite timescale of transport/mixing in the ocean, e.g., Skinner and Shackleton, 2005). However, the fact that they broadly parallel each other during *both* glacial intervals lends credibility to our chronostratigraphy.

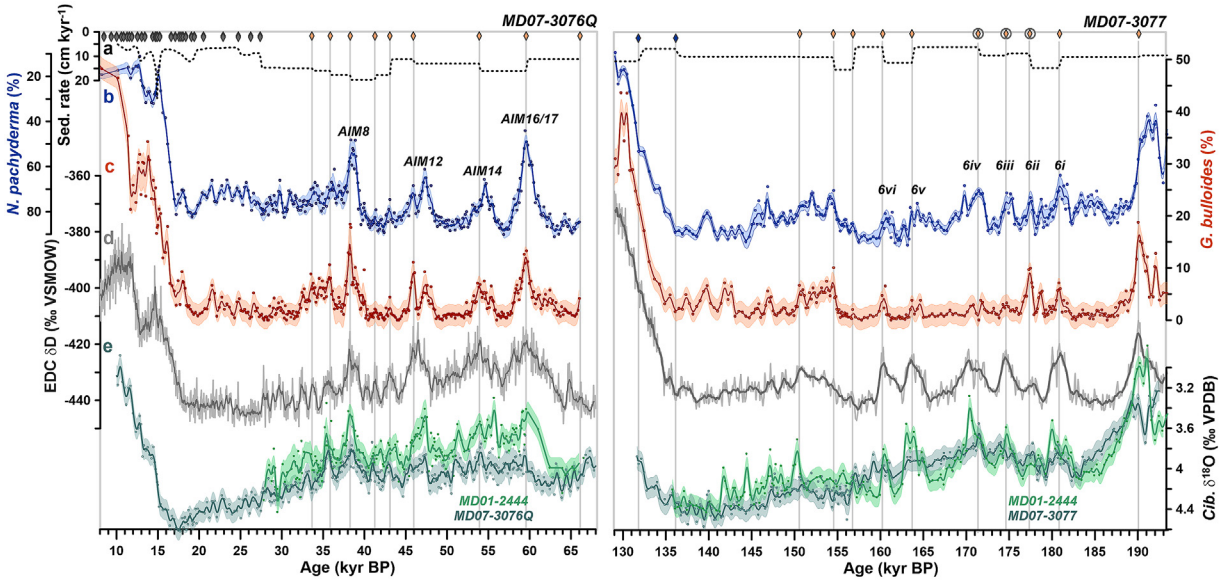

Fig. 2. Chronologies of sediment cores MD07-3076Q (Termination (T) I and Marine Isotope Stage (MIS) 3, left) and MD07-3077 (TII and MIS 6, right). (a) Sedimentation rate (line) and tiepoints (^{14}C dates (grey), alignment of abundance variations of *G. bulloides* (orange) and *N. pachyderma* (blue) with EPICA Dome C (EDC) δD; Gottschalk et al., 2016b; Channell et al., 2017), (b) abundance changes of *N. pachyderma*, (c) abundance changes of *G. bulloides*, (d) EDC δD (Jouzel et al., 2007) shown on the AICC2012 chronology (Bazin et al., 2013; Veres et al., 2013) and (e) *C. kullenbergi* $\delta^{18}O$ records in comparison to mean benthic $\delta^{18}O$ records from the Iberian margin (MD01-2444; Skinner et al., 2007; Margari et al., 2010). Lines and envelopes in (b), (c) and (e) show 500 yr-running averages and 2σ-uncertainties, respectively. Encircled symbols show adjusted age markers that differ from the chronology published in Channell et al. (2017), as described in the text. The annotation of Antarctic warming events (AIM – Antarctic Isotope Maxima) follows EPICA Community Members (2006) for MIS 3 and Margari et al. (2010) for MIS 6.

Please cite this article as: Gottschalk, J et al., Southern Ocean link between changes in atmospheric CO_2 levels and northern-hemisphere climate anomalies during the last two glacial periods, Quaternary Science Reviews, https://doi.org/10.1016/j.quascirev.2019.106067

3.6. Antarctic ice core $CO_{2,atm}$ data

In order to evaluate the possible influence of changes in the deep ocean carbon inventory on $CO_{2,atm}$, we compare available high-resolution $CO_{2,atm}$ records, as compiled by Bereiter et al. (2015), with our marine proxy data on millennial timescales. The mean temporal resolution of the available ice core $CO_{2,atm}$ data covering MIS 3 from 63 to 32 kyr BP (~160±130 yr, n = 197) (Bereiter et al., 2012; Ahn and Brook, 2014) is much higher than during MIS 6 from 183 to 134.5 kyr BP (~1400±700 yr, n = 34) (Petit et al., 1999; Schneider et al., 2013), hampering a comparison of the $CO_{2,atm}$ variability during MIS 6 to our centennially resolved proxy data (220 ± 70 yr, n = 220). In order to circumvent this limitation, we predict millennial-scale $CO_{2,atm}$ variations by taking advantage of the close relationship between the Antarctic temperature proxy δD and $CO_{2,atm}$ (Petit et al., 1999; Fischer et al., 2010). We obtain separate linear regressions between EDC δD (smoothed by a 500 yr-running average; Jouzel et al., 2007) and $CO_{2,atm}$ for MIS 3 and MIS 6 using the compilation of Bereiter et al. (2015) (Fig. 3). Our regression for MIS 3 shows a correlation coefficient of (R^2=0.64) (p<0.05), whereas R^2 for the MIS 6 regression is lower (R^2=0.41, p<0.05, excluding two outliers; Fig. 3). Both are statistically significant. The resulting 2σ-uncertainty of the predicted $CO_{2,atm}$ (hereafter referred to as $CO_{2,atm\text{-}PRED}$) is 10 ppm and 12 ppm, respectively (Fig. 3).

The ice-core records available for MIS 3 and MIS 6 suggest a difference in the baseline of $CO_{2,atm}$, with overall lower values during MIS 6 mainly derived from the Vostok ice core (Fig. 3). However, known offsets in absolute $CO_{2,atm}$ levels among different ice cores, for instance in the case of glacial $CO_{2,atm}$ records (Bereiter et al., 2012; Eggleston et al., 2016), suggest that the difference in MIS 3-to-MIS 6 $CO_{2,atm}$ baselines might be an artefact driven by in-situ production of CO_2. As such offsets still lack a coherent explanation, absolute differences smaller than 5–10 ppm in $CO_{2,atm}$ should be interpreted with caution. Nonetheless, given the low resolution of $CO_{2,atm}$ data during MIS 6 (Petit et al., 1999; Bereiter et al., 2015), we consider MIS 6 $CO_{2,atm\text{-}PRED}$ changes as a reasonable first-order approximation of $CO_{2,atm}$ variability during that time period. High-resolution $CO_{2,atm}$ data from Antarctic ice cores during MIS 6 are needed to test the reliability of this approach.

4. Results

4.1. Changes in bottom water oxygenation

We observe systematic changes in the enrichment of U in authigenic coatings of foraminifera, which track past variations in Antarctic temperature and $CO_{2,atm(\text{-}PRED)}$ (Fig. 4). Bulk foraminifer U/Mn- and U/Ca ratios closely resemble each other both during MIS 3 and MIS 6 (Supplementary Fig. S2). If foraminiferal coating U and Mn enrichment is respectively driven by precipitation of uraninite and Mn-oxides under anoxic and oxic conditions , bulk foraminifer U/Ca- and Mn/Ca ratios are expected to anticorrelate (Boiteau et al., 2012). If their enrichment occurs below the anoxic boundary, they are expected to correlate with one another (Detlef et al., 2020; Skinner et al., 2019). U/Ca- and Mn/Ca ratios of our planktonic foraminifer samples show a statistically significant positive regression slope (*G. bulloides:* n = 96; *G. inflata:* n = 237; Supplementary Fig. S2), suggesting that they were governed by similar processes. In contrast, *Uvigerina* spp. do not show a strong relationship between U and Mn enrichment (if at all a slight anti-correlation; Supplementary Fig. S2), potentially highlighting the opposing redox-behaviour of these two elements. However, irrespective of whether Mn/Ca and U/Ca are correlated or anti-correlated, relative changes in the foraminiferal U/Ca- and U/Mn ratios agree (Supplementary Fig. S2), suggesting that the redox-sensitive U precipitation is the main control of the observed changes in foraminiferal U/Ca- and U/Mn ratios.

During MIS 3 and TI, *G. bulloides* and *Uvigerina* spp. U/Mn ratios and the $\delta^{13}C_{Ck\text{-}Ga}$ gradient show marked variations during strong Antarctic warming events (AIM 8, 12, 14, 16/17), as well as during the more subdued AIM 6 and 7 (*sensu* EPICA Community Members, 2006, Figs. 4 and 5). Both bottom water oxygenation records parallel changes in $CO_{2,atm}$ levels, indicating an increase in bottom water oxygenation in the deep sub-Antarctic Atlantic during rising $CO_{2,atm}$ (Figs. 4 and 5). The relative change in *G. bulloides* and

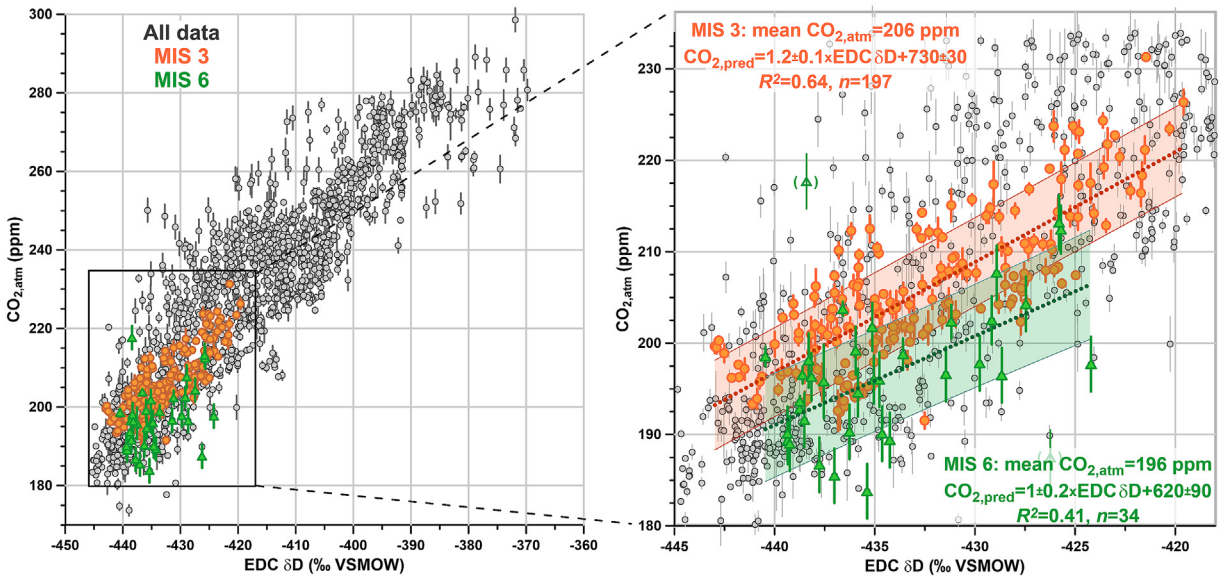

Fig. 3. Prediction of atmospheric CO_2 levels ($CO_{2,atm\text{-}PRED}$) during MIS 6 based on δD variations in the EDC ice core. Linear regression model between EDC δD (Jouzel et al., 2007) and $CO_{2,atm}$ concentrations (Bereiter et al., 2015) for 63-32 kyr BP (MIS 3, orange: $CO_{2,atm\text{-}PRED}$ = 1.2 ± 0.1 × (EDC δD)+730 ± 30) and for 183-134.5 kyr BP (MIS 6, green: $CO_{2,atm\text{-}PRED}$ = 1.0 ± 0.2 × (EDC δD)+620 ± 90), excluding two bracketed outliers), used to predict $CO_{2,atm}$ during MIS 3 and MIS 6, respectively. Grey symbols show all ice core data from 800 to 2 kyr BP. Envelopes (right) show the 1σ-uncertainties of the regression models.

Please cite this article as: Gottschalk, J et al., Southern Ocean link between changes in atmospheric CO_2 levels and northern-hemisphere climate anomalies during the last two glacial periods, Quaternary Science Reviews, https://doi.org/10.1016/j.quascirev.2019.106067

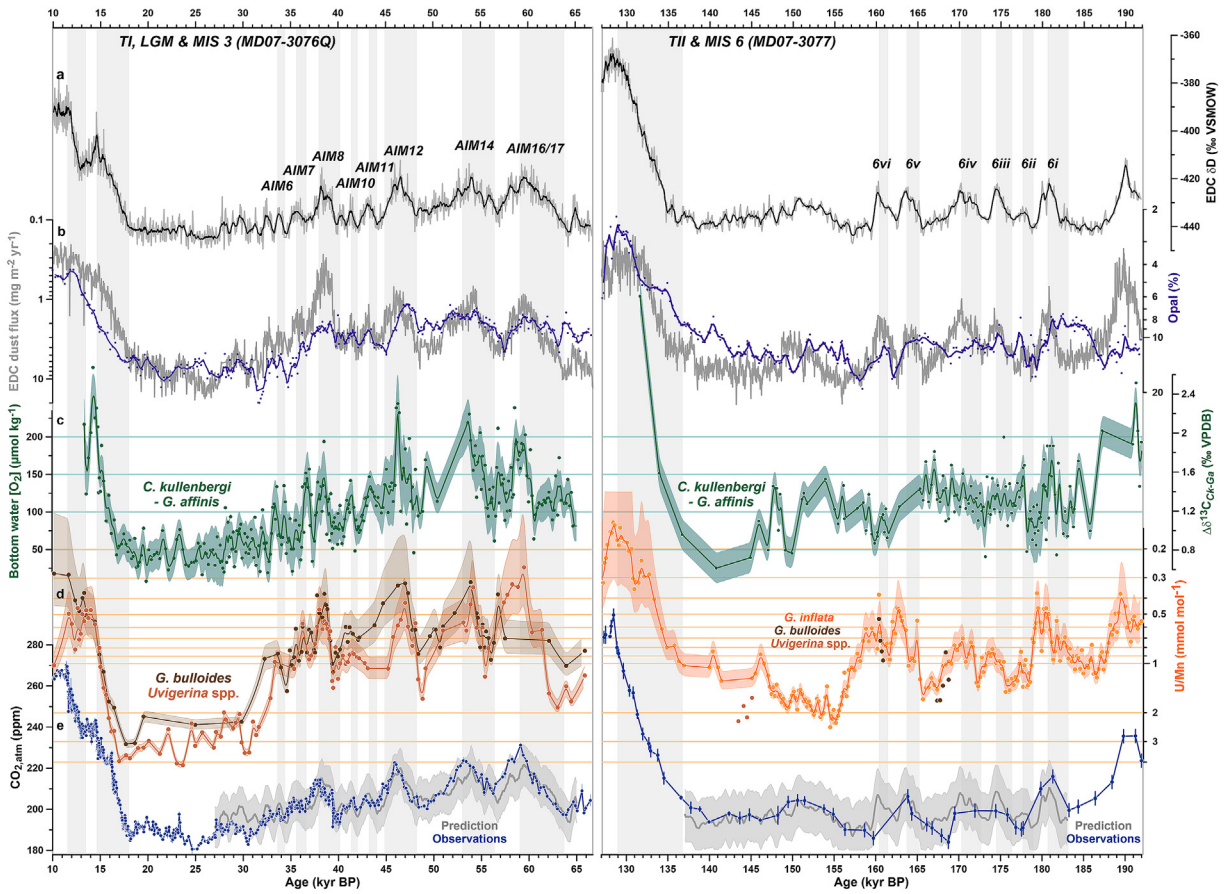

Fig. 4. Deep-ocean oxygenation- and productivity changes in the South Atlantic during TI and MIS 3 (left, MD07-3076Q), and TII and MIS 6 (right, MD07-3077). (a) EDC δD (Jouzel et al., 2007), (b) EDC dust fluxes (grey; Lambert et al., 2012) and sedimentary opal content at our study site (purple, corrected for incomplete water removal as shown in Supplementary Figs. S1), (c) gradient between *C. kullenbergi* (*Ck*) $\delta^{13}C$ and *G. affinis* (*Ga*) $\delta^{13}C$, $\Delta\delta^{13}C_{Ck\text{-}Ga}$, and corresponding bottom water $[O_2]$ after Hoogakker et al. (2015), see Supplementary Fig. S3 for individual benthic foraminifer $\delta^{13}C$ records, (d) U/Mn ratios of *G. bulloides* (dark brown), *Uvigerina* spp. (light brown) and *G. inflata* (orange) (cf. foraminiferal U/Ca ratios in Supplementary Figs. S2) and (e) observed $CO_{2,atm}$ variations (dark blue; Bereiter et al., 2015) and $CO_{2,atm}$ variations predicted from EDC δD (grey line with 1σ-envelope; cf. Fig. 3) for MIS 3 (left) and MIS 6 (right). Lines and envelopes in (b) to (d) represent 500 yr-running averages and 1σ-uncertainties, respectively. The lower uncertainty range of *G. inflata* U/Mn is truncated at 0.08 mmol mol^{-1}. Grey bars indicate intervals of rising $CO_{2,atm(\text{-PRED})}$.

Uvigerina spp. U/Mn levels correlates with the magnitude of parallel $CO_{2,atm}$ variations (Fig. 6a). During the penultimate glacial period (i.e., AIM 6vi to i, *sensu* Margari et al., 2010), changes in *G. inflata* U/Mn ratios are similar to Antarctic temperature variations (Figs. 4 and 5). Decreases in *G. inflata* U/Mn levels during Antarctic warming events coincide with increases in $CO_{2,atm\text{-}PRED}$ levels during MIS 6 (Figs. 4 and 5).

We estimated the maximum magnitudes of foraminiferal U/Mn change during intervals of Antarctic warming as defined in Margari et al. (2010) and link them with maximum parallel rises in $CO_{2,atm}$ that we consider to be associated with (see Fig. 5). Intervals of U/Mn change, $CO_{2,atm(\text{-PRED})}$ rise and Antarctic warming do not necessarily fully agree in their timing. In fact, during Dansgaard-Oeschger (DO) stadials 14 and DO16/17 as well as stadials associated with 6iv and 6ii, the U/Mn maximum occurs slightly later than the onset of Antarctic warming (Fig. 5f). Similarly, intervals of rising $CO_{2,atm}$ levels during MIS 3 (e.g., DO14 and DO16/17) may last slightly longer than the period of rising temperatures over Antarctica (Fig. 5g). The relationship between foraminiferal U/Mn- and $CO_{2,atm(\text{-PRED})}$ changes during stadial conditions is the same during both glacial periods (Fig. 6a).

Distinct excursions of *G. affinis* $\delta^{13}C$ from *C. kullenbergi* $\delta^{13}C$ during MIS 3 (Supplementary Fig. S3) indicate that the observed bottom water $[O_2]$ change in parallel with variations in foraminiferal U/Mn amounts to 110 ± 50 μmol kg^{-1} on average (Fig. 4; Gottschalk et al., 2016a). Although the U/Mn proxy seems to provide the most consistent pattern of variability between the last two glacials, its agreement with $\Delta\delta^{13}C_{Ck\text{-}Ga}$-based bottom water $[O_2]$ variations during MIS 6 is quite poor (Fig. 4). As the $\Delta\delta^{13}C_{Ck\text{-}Ga}$ proxy is based on the *aerobic* respiration of organic matter in marine sub-surface sediments, one can surmise that strong carbon fluxes to the sea floor may have caused *anaerobic* organic matter degradation in sub-surface sediments to severely bias the proxy (Jacobel et al., 2019). This might have been the case during MIS 6, but not during MIS 3. Furthermore, the $\Delta\delta^{13}C_{Ck\text{-}Ga}$ proxy relies on an accurate recording of pore-water $\delta^{13}C$ at the anoxic boundary in sub-surface sediments via the deep-infaunal benthic foraminifera *G. affinis*, and of bottom water $\delta^{13}C$ levels by the benthic foraminifer *C. kullenbergi*. Either or both of these conditions might not have been met during MIS 6: firstly, *Globobulimina* species and other deep infaunal benthic foraminifera were shown to be capable of denitrification, and can hence thrive significantly below the anoxic boundary, where pore water $\delta^{13}C$ is lowered independently of $[O_2]$ (Risgaard-Petersen et al., 2006; Piña-Ochoa et al., 2010; Glock et al., 2019); and secondly, *C. kullenbergi* was suggested to live and possibly prefer slightly infaunal habitats with lower $\delta^{13}C$ than in bottom waters (Gottschalk et al., 2016b). Along with large intra-species $\delta^{13}C$ variability and potential vital effects of both benthic

Please cite this article as: Gottschalk, J et al., Southern Ocean link between changes in atmospheric CO_2 levels and northern-hemisphere climate anomalies during the last two glacial periods, Quaternary Science Reviews, https://doi.org/10.1016/j.quascirev.2019.106067

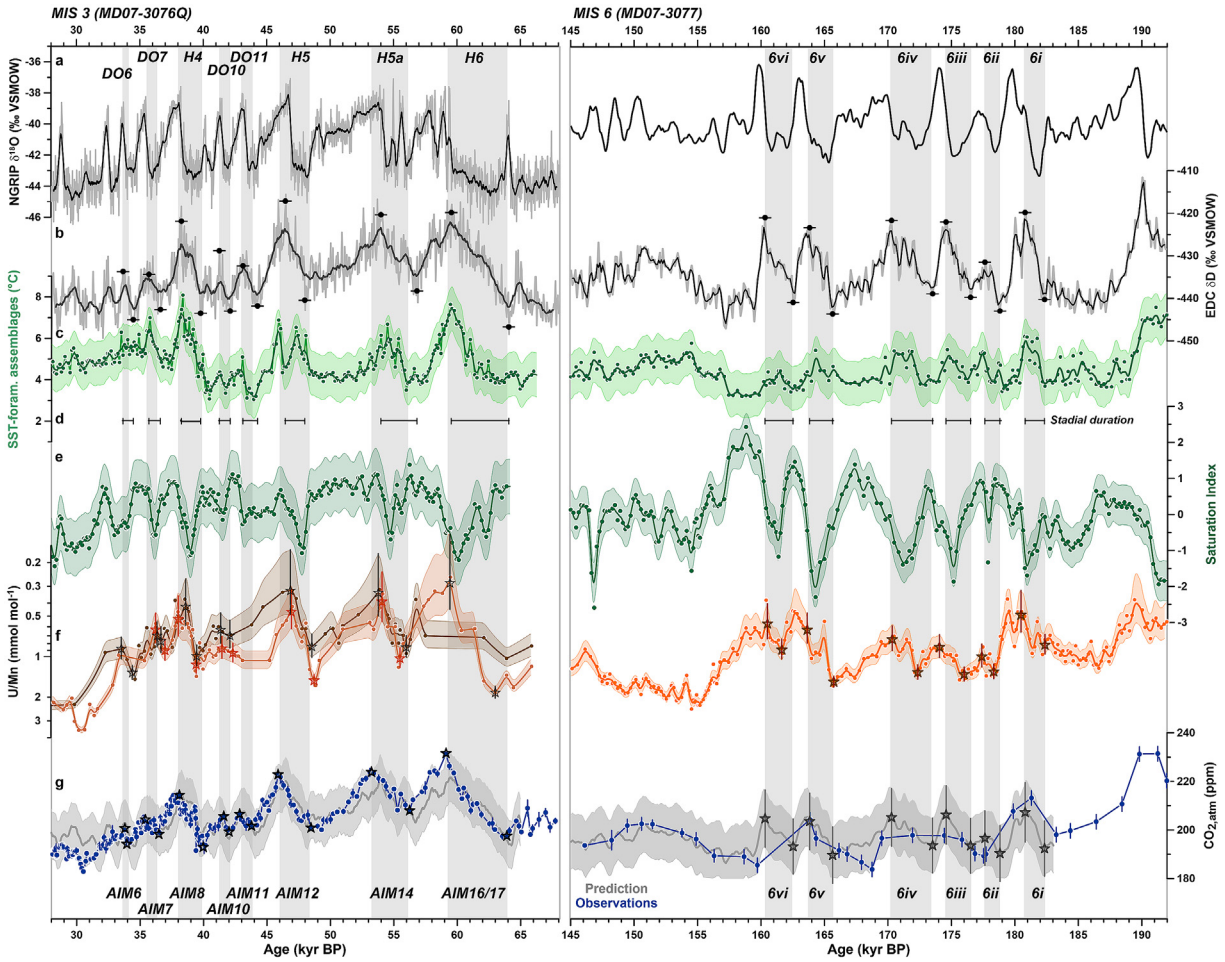

Fig. 5. Millennial-scale $CO_{2,atm}$ variations compared to changes in carbonate saturation and bottom water oxygenation in the deep sub-Antarctic Atlantic during MIS 3 (left, MD07-3076Q) and MIS 6 (right, MD07-3077). (a) Observed (MIS 3: NGRIP members, 2004) and predicted NGRIP $\delta^{18}O$ variations (MIS 6: Barker et al., 2011), (b) EDC δD (grey; Jouzel et al., 2007) and symbols highlighting the onset and ends of northern-hemisphere stadials according to Margari et al. (2010) (black), (c) summer sea surface temperatures (green; SST) derived from planktonic foraminiferal assemblage counts in the study cores and the calibration of Haddam et al. (2016), (d) stadial durations (i.e., duration of Antarctic warming), according to Margari et al. (2010), (e) saturation index as defined in Gottschalk et al., 2015a and shown in Supplementary Fig. S4, (f) authigenic-coating U/Mn ratios of *G. bulloides* (dark brown), *Uvigerina* spp. (light brown) and *G. inflata* (orange), stars indicate onsets and ends of gradual U/Mn change associated with northern-hemisphere stadials, (g) observed $CO_{2,atm}$ concentrations (dark blue; Bereiter et al., 2015) and $CO_{2,atm\text{-}PRED}$ (grey, cf. Fig. 3), stars indicate onsets and ends of $CO_{2,atm(\text{-}PRED)}$ change associated with northern-hemisphere stadials. Grey bars indicate intervals of rising $CO_{2,atm(\text{-}PRED)}$ levels. Annotations of Dansgaard-Oeschger (DO) stadials, Heinrich (H) events and AIMs follow Dansgaard et al. (1993), Hemming (2004), EPICA Community Members (2006) and Margari et al. (2010), respectively.

foraminifer species, as well as carbonate dissolution changing the pore-water $\delta^{13}C$ gradient, these processes may have conspired to cause a reduced sensitivity of the $\Delta\delta^{13}C$ proxy to bottom water $[O_2]$ changes during MIS 6. The apparent discrepancy of our MIS 6 $\Delta\delta^{13}C_{Ck\text{-}Ga}$ data underlines possible differences in glacial climate background conditions but also emphasises the need for further work investigating the controls on both the $\Delta\delta^{13}C_{Ck\text{-}Ga}$ and U/Mn redox proxies under a wide range of depositional and hydrographic settings.

4.2. Changes in the carbonate saturation state of the deep sub-Antarctic Atlantic Ocean

The carbonate saturation index (and all individual partial sedimentary dissolution proxies; Supplementary Fig. S4) exhibits several minima during MIS 3 and MIS 6 consistent with the presence of corrosive bottom waters in the deep sub-Antarctic Atlantic, likely of southern origin (Fig. 5; Gottschalk et al., 2015a). This is also consistent with quantitative bottom water $[CO_3^{2-}]$ variations at the study site during MIS 3 (Supplementary Fig. S4; Gottschalk et al., 2015a). The saturation index minima are paralleled by gradually decreasing foraminiferal U/Mn ratios (Fig. 5), and coincide with minima in epibenthic foraminiferal $\delta^{13}C$, and hence stadial conditions, at the Iberian Margin (Fig. 7; Skinner et al., 2007; Margari et al., 2010).

The duration of northern-hemisphere stadials is expressed in the length of parallel Antarctic warming (Margari et al., 2010). By construction, SST at the core site closely varies with Antarctic temperature, and we hence compare the duration of Antarctic warming, i.e., the length of northern-hemisphere stadials, with the maximum amplitude of foraminiferal U/Mn change that we consider is associated with it (see Fig. 5; Margari et al., 2010). We find that the magnitude of change in foraminiferal U/Mn ratios during both glacial periods linearly correlates with the duration of northern-hemisphere stadial conditions (Fig. 6b). A difference between the two glacial relationships cannot be identified (Fig. 6b).

Furthermore, the presence of corrosive bottom waters at our core site (i.e., low saturation indices) parallels intervals of rising $CO_{2,atm(\text{-}PRED)}$ levels (Fig. 5). Relying on MIS 6 $CO_{2,atm\text{-}PRED}$ levels and ice core observations during MIS 3 (Bereiter et al., 2015), we

Please cite this article as: Gottschalk, J et al., Southern Ocean link between changes in atmospheric CO_2 levels and northern-hemisphere climate anomalies during the last two glacial periods, Quaternary Science Reviews, https://doi.org/10.1016/j.quascirev.2019.106067

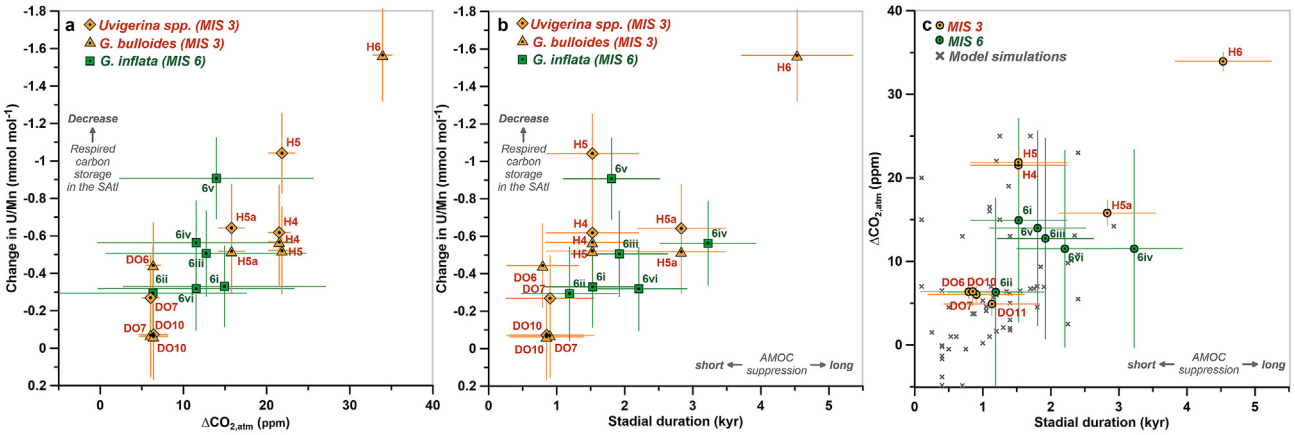

Fig. 6. Variations in $CO_{2,atm}$ levels during stadials and associated changes in respired carbon content at our study site. (a) Change in foraminiferal U/Mn versus parallel change in $CO_{2,atm}$ (i.e., based on observations in MIS 3 and our MIS 6 prediction), (b) change in foraminiferal U/Mn ratios versus the duration of northern hemisphere stadials following Margari et al. (2010) and (c) change in $CO_{2,atm}$ (i.e., based on observations in MIS 3 and our MIS 6 prediction) versus the duration of stadial conditions (circles). In (c) we also compare our proxy data with simulated $CO_{2,atm}$ changes during stadials in freshwater hosing experiments in the North Atlantic (crosses; see review of Gottschalk et al., 2019). Data based on *G. inflata*, *Uvigerina* spp. and *G. bulloides* are shown as squares, diamonds and triangles, respectively. Time intervals are annotated as in Fig. 5. AMOC – Atlantic Meridional Overturning Circulation; SAtl – South Atlantic.

observe a good correlation between the duration of these stadials and the magnitude of concomitant $CO_{2,atm(-PRED)}$ increase (Fig. 6c). No significant difference in the relationship between the two can be identified during MIS 3 and MIS 6 (Fig. 6c).

4.3. Changes in opal percentages

During MIS 3 and TI, changes in sedimentary opal percentages in MD07-3076Q broadly co-vary with EDC dust fluxes (Fig. 4; Gottschalk et al., 2016a). This relationship could suggest an influence of aeolian dust-driven iron fertilisation on nutrient utilisation and export production in the sub-Antarctic Zone during the last glacial period (Martin, 1990; Anderson et al., 2014; Lamy et al., 2014; Martínez-García et al., 2014; Gottschalk et al., 2016a). In contrast, during MIS 6 and TII, the link between opal percentages and EDC dust variations is rather poor on millennial timescales, and significant offsets exist between changes in the sedimentary opal content at our study site and the EDC dust flux record (Fig. 4).

4.4. Ice-rafted debris

The abundance of IRD in our study core during the first half of MIS 3 is low but progressively increases towards the end of MIS 3, with pronounced peaks during North Atlantic stadials, and periods of Antarctic warming (Fig. 7). IRD percentages were generally higher during MIS 6 than during MIS 3, and show a more distinct response during stadials (Fig. 7). Kanfoush et al. (2000) interpreted IRD peaks in the South Atlantic as indication of significant iceberg fluxes to the South Atlantic. In contrast, Nielsen et al. (2007) highlighted that a large proportion of the IRD material in the South Atlantic identified by Kanfoush et al. (2000) was likely transported from the South Sandwich and Bouvet Islands via sea ice.

5. Discussion

5.1. Changes in deep South Atlantic carbon sequestration during the last two glacial periods

Our foraminiferal U/Mn records spanning MIS 3 and MIS 6 indicate increases in bottom water oxygenation in the deep South Atlantic during North Atlantic stadials, which we argue indicates changes in the respired carbon content of the deep South Atlantic (Gottschalk et al., 2016a; this study). During MIS 3, these occur in parallel to reductions in the sedimentary opal content (Fig. 4), rising SSTs (Fig. 5) and increased ice-rafting/-export (Fig. 7; Gottschalk et al., 2016a; this study). This also applies to MIS 6, with the exception of distinct offsets between variations in opal, Antarctic dust fluxes and deep South Atlantic bottom water oxygen changes (Fig. 4).

During MIS 3, variations in the degree of iron fertilisation via aeolian dust supply were suggested to control export production, and hence opal fluxes, in the glacial sub-Antarctic Atlantic (Anderson et al., 2014a; Martínez-García et al., 2014), contributing to millennial-scale bottom water oxygen and respired carbon changes at depth (Gottschalk et al., 2016a; Jaccard et al., 2016). However, whether the same mechanism operated during MIS 6 remains ambiguous (Fig. 4). The observed opal changes during MIS 6 may not be driven by aeolian dust supply (iron fertilisation), or sedimentary opal percentages may poorly represent annually integrated export production (of all taxonomic groups) in the sub-Antarctic Atlantic during that time interval. Indeed, the opal content in marine sediments was shown to be influenced by the availability of silicic acid, Antarctic sea ice extent, ecosystem structures and the degree of diatom silicification causing variable Si:C ratios of exported material (Chase et al., 2015). Irrespective of whether our opal data in MIS 6 faithfully record changes in export production, we argue, based on our proxy records and earlier findings (Gottschalk et al., 2016a), that increased ventilation of the deep Southern Ocean must be invoked to explain increased bottom water oxygen levels in the deep South Atlantic during intervals of Antarctic warming (e.g., Skinner et al., 2010, 2014; Gottschalk et al., 2015ab, Gottschalk et al., 2016a; Jaccard et al., 2016). Southern Ocean ventilation was likely accompanied by increased air-sea CO_2 equilibration and adjusted surface ocean buoyancy forcing in the Antarctic Divergence Zone of the Southern Ocean, driving up both $CO_{2,atm}$ levels and deep Southern Ocean oxygenation (Anderson et al., 2009; Skinner et al., 2010, 2014; Gottschalk et al., 2015ab, Gottschalk et al., 2016a; Jaccard et al., 2016). These changes were likely linked to variations in deep-ocean respired carbon content in other ocean basins, such as the Atlantic and the Pacific Ocean (e.g., Jaccard et al., 2009; Menviel et al., 2015a, 2018; Umling and Thunell,

Please cite this article as: Gottschalk, J et al., Southern Ocean link between changes in atmospheric CO_2 levels and northern-hemisphere climate anomalies during the last two glacial periods, Quaternary Science Reviews, https://doi.org/10.1016/j.quascirev.2019.106067

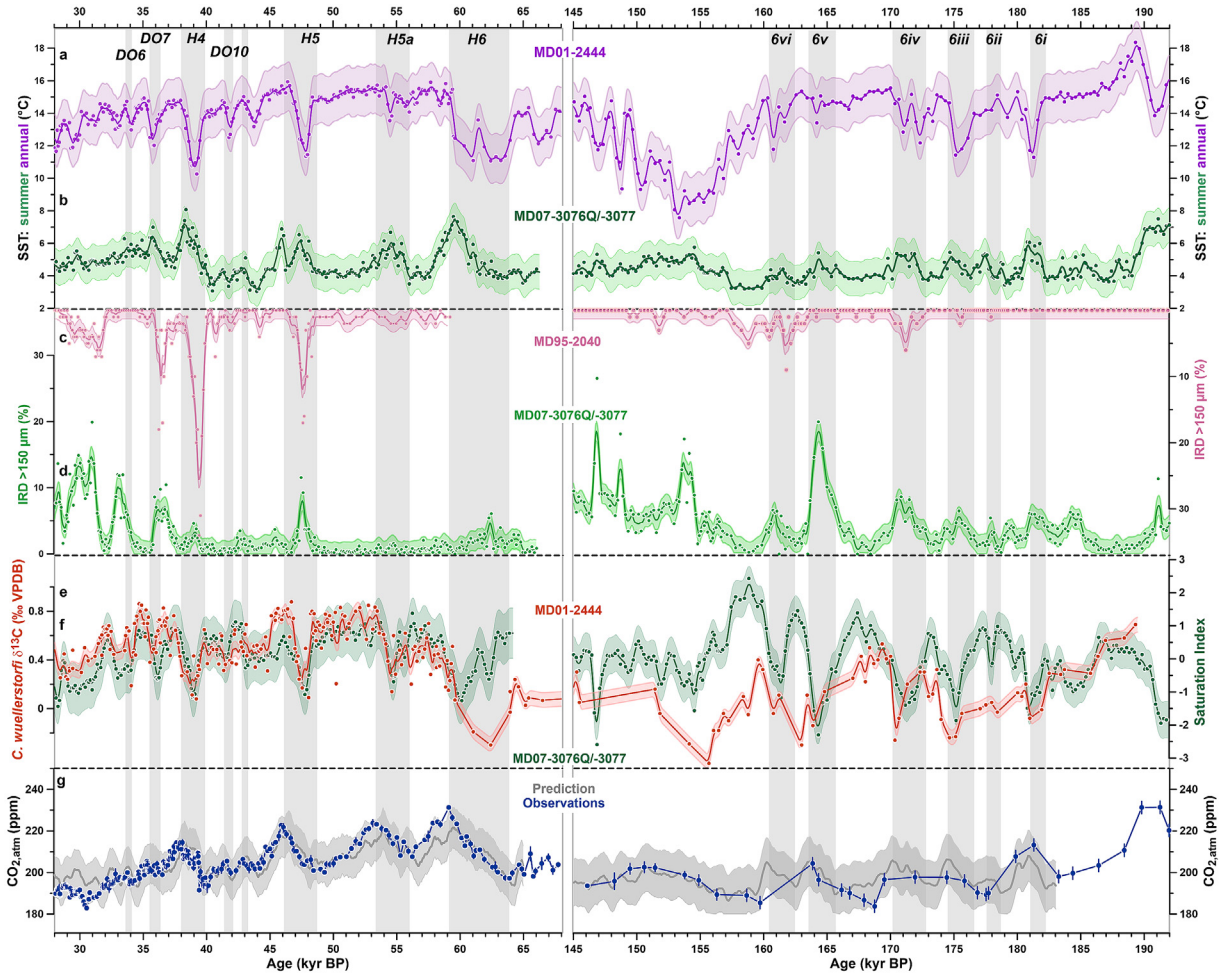

Fig. 7. Comparison of climate variability in the South Atlantic and the North Atlantic (Iberian margin) during MIS 3 (left) and MIS 6 (right). SST variability reconstructed in (a) sediment core MD01-2444 based on alkenone unsaturation indices (annual mean; Martrat et al., 2007) and (b) MD07-3076Q/-3077 based on planktonic foraminiferal assemblage counts (summer; this study), changes in the abundance of ice-rafted debris (IRD) in (c) MD95-2040 (de Abreu et al., 2003; age model based on Margari et al., 2010) and (d) MD07-3076Q/-3077 (this study), changes in the variability of the Atlantic Meridional Overturning Circulation (AMOC) recorded in (e) epibenthic foraminiferal (*C. wuellerstorfi*) $\delta^{13}C$ changes in core MD01-2444 (2.6 km water depth) (brown; Skinner et al., 2007; Margari et al., 2010), (f) carbonate saturation indices in core MD07-3076Q/-3077 (green; Gottschalk et al., 2015a; this study), and (g) observed (dark blue; Bereiter et al., 2015) and predicted $CO_{2,atm}$ levels (grey; this study). Vertical bars highlight intervals of rising $CO_{2,atm(-PRED)}$ concentrations. Solid lines and error envelopes show 500 yr-running averages. The error envelopes refer to 1σ-calibration uncertainties: (a) 1.5 °C (Martrat et al., 2007), (b) ~1 °C (this study), 1σ-uncertainties of the IRD counts, i.e., (c) 1.5% (conservative estimate; de Abreu et al., 2003) and (d) 1.5% (this study), (e) the external $\delta^{13}C$ reproducibility of carbonate standards (1σ = 0.06‰), (f) the 1σ-uncertainties of the saturation index, and (g) the 1σ-uncertainties of predicted $CO_{2,atm}$ (~12 ppm, cf. Fig. 3). All data are shown on the GICC05 or equivalent AICC2012 age scales.

2017; Anderson et al., 2019; Chalk et al., 2019). Hence, we suggest that similar mechanisms of (southern high-latitude) oceanic CO_2 release might have operated during the last two glacial periods, which is supported by similar patterns of reconstructed bottom water oxygenation change at our study site and parallel $CO_{2,atm(-PRED)}$ rise (Fig. 6a).

The occurrence of saturation index minima in the deep South Atlantic during intervals of increasing bottom water oxygenation (Fig. 5) indicates a shallower cell and/or reduced southward advection of NADW, favouring the presence of southern-sourced (carbonate ion-undersaturated) water masses at our core site, as suggested previously (Gottschalk et al., 2015a). This is supported by an agreement of our saturation index with epibenthic $\delta^{13}C$- (Skinner et al., 2007; Margari et al., 2010) and SST changes at the Iberian Margin (Martrat et al., 2007, Fig. 7), the high-resolution $^{231}Pa/^{230}Th$ record from Bermuda Rise (Henry et al., 2016) and a carbonate saturation record from the deep Cape Basin (Gottschalk et al., 2018), which reflect similar AMOC changes in the Atlantic basin. This agreement corroborates a strong causal link between bottom water $[O_2]$ changes in the deep South Atlantic and end-member changes of southern-sourced water masses related to variations in air-sea gas exchange- and/or the ventilation rate, which may be linked to variations in the southward extent of NADW.

However, this may be challenged by the observation of increasing bottom water oxygenation (i.e., decreasing respired carbon levels) in deep South Atlantic during periods of rising $CO_{2,atm}$ levels, despite low $[CO_3^{2-}]$ levels (i.e., saturation index minima) (Fig. 5), whereas a positive correlation between bottom water $[CO_3^{2-}]$ and -oxygenation is expected. Our saturation index in fact shows an initial drop at the stadial onset and a subsequent gradual increase towards the end of the stadial (Fig. 5). Changes in bottom water $[O_2]$ and $[CO_3^{2-}]$ may be affected by different processes operating on different timescales, involving not only changes in the amount of respired carbon, but also changing northern- and southern-sourced end-member signatures and/or -contributions. A decrease in the contribution of northern-sourced water masses might have strongly affected bottom water $[CO_3^{2-}]$ levels *at the onset*

Please cite this article as: Gottschalk, J et al., Southern Ocean link between changes in atmospheric CO_2 levels and northern-hemisphere climate anomalies during the last two glacial periods, Quaternary Science Reviews, https://doi.org/10.1016/j.quascirev.2019.106067

of stadial conditions, when differences in bottom water [O_2] between northern- and southern-sourced water masses might have been small, thus explaining the absence of abrupt changes in our U/Mn-based bottom water [O_2] record. *During* North Atlantic stadials, however, increasing equilibration of southern-sourced water masses with the atmosphere and increased AABW formation might have rapidly affected bottom water [O_2] but more slowly [CO_3^{2-}], because the equilibration time of the carbonate system is an order of magnitude longer compared to non-dissociating gases. Further sensitivity tests using numerical models and/or further spatial coverage across the Atlantic are required to test this hypothesis.

5.2. Inter-hemispheric climate variability and changes in deep-ocean carbon storage during the last two glacial periods

The exact mechanisms that connect the hemispheres over deglaciations or millennial-scale climate events, and their implications for ocean respired carbon storage and $CO_{2,atm}$ change, remain difficult to determine. However, insights into the controls on deep-ocean respired carbon storage in the deep South Atlantic may emerge from a comparison of millennial events occurring under different background climate states during MIS 3 and MIS 6 (sections 5.2.1 and 5.2.2) and from a comparison of our proxy data with numerical model outputs (sections 5.2.3 and 5.2.4).

5.2.1. Role of glacial background conditions

We observe slightly higher foraminiferal U/Mn ratios (indicative of lower [O_2] and higher respired carbon levels) during MIS 6 (mean U/Mn = 1.12 mmol mol^{-1}, 183–143.5 kyr BP) than during MIS 3 (mean U/Mn = 0.75 mmol mol^{-1}, 63-32 kyr BP) (Fig. 4). This may be associated with differences in the foraminiferal species used for the U/Mn analyses during both glacial periods, but a few *G. bulloides* and *Uvigerina* spp. analyses during MIS 6 show agreement or slightly higher values than the *G. inflata* data (Fig. 4), which supports our observation. Although this needs to be tested with further proxy data, our observations may suggest overall more intense respired carbon sequestration in the deep South Atlantic during MIS 6 compared to MIS 3. In contrast, our $\Delta\delta^{13}C$-derived [O_2] data suggest similar bottom water oxygenation, and hence respired carbon levels, during these two glacial periods (Fig. 4). However, this [O_2] proxy may be biased during MIS 6, as discussed above.

Based on North Atlantic epibenthic $\delta^{13}C$ data, Margari et al. (2010) argued for a shallower AMOC cell during MIS 6 than during MIS 3. This may have promoted an expansion of southern-sourced water masses, and may have hampered mid-depth mixing with overlying (northern-sourced) water masses, more so during MIS 6 than during MIS 3, owing to increased distance from rough topography (Adkins, 2013; Ferrari et al., 2014), or an increased density difference between the two. This slightly different water mass structure in the Atlantic and Southern Ocean during MIS 6 may have caused overall increased carbon sequestration in the deep South Atlantic and the Southern Ocean compared to MIS 3, and possibly also lower $CO_{2,atm}$ levels. This is supported by numerical model simulations that highlight an increased carbon sequestration potential of the ocean through a combined weakening of the overturning rate of both NADW and AABW (Menviel et al., 2017; Ödalen et al., 2018).

In addition, we find increased variability in IRD supply to the central South Atlantic and overall cooler SST conditions during MIS 6 than during MIS 3 (Fig. 7). Our data are consistent with a more proximal seasonal sea ice edge to the study site and/or an increased production of icebergs, which would suggest more extensive sea ice cover and generally colder conditions in the Southern Ocean during MIS 6 (Fig. 7). Along with associated changes in Southern Ocean buoyancy forcing, more extended Antarctic sea ice cover during MIS 6 may have contributed to stronger respired carbon storage during MIS 6 compared to MIS 3, as long as this reduced ocean-to-atmosphere CO_2 fluxes (Stephens and Keeling, 2000) more than it reduced atmosphere-to-ocean CO_2 fluxes due to diminished biological export production (Kurahashi-Nakamura et al., 2007; Sun and Matsumoto, 2010). Overall, our findings suggest that the difference in glacial boundary conditions, specifically through impacts on water mass geometries in the Atlantic (as indicated by Iberian margin benthic $\delta^{13}C$ values) and Antarctic surface buoyancy forcing (as shown by IRD abundances at our study site) likely accounted for differences in deep ocean carbon storage, and possibly for differences in $CO_{2,atm}$ background levels during MIS 3 and MIS 6 (Fig. 3).

5.2.2. Stadial duration and atmospheric CO_2 rise

Intervals of rising bottom water oxygenation, and hence decreasing respired carbon levels in the deep South Atlantic, coincide with periods of weakened AMOC, i.e., northern-hemisphere stadials, during the last two glacial periods (Fig. 4). The tight relationship between the duration of northern-hemisphere stadials and the magnitude of concomitant bottom water oxygen increase at our core site (Fig. 6b) suggests that respired carbon is gradually lost from the deep South Atlantic during AMOC perturbations. The associated millennial adjustment timescale may reflect the influence of Southern Ocean vertical mixing and deep-ocean turnover rather than fast (centennial-scale) adjustments in the terrestrial biosphere. The observed link between deep South Atlantic oxygen/respired carbon changes and $CO_{2,atm(-PRED)}$ variations (Fig. 6a) suggests that the time the AMOC remains suppressed largely defines the net CO_2 flux from the ocean to the atmosphere, thus determining the magnitude of $CO_{2,atm}$ increase during northern-hemisphere stadials (Fig. 6c).

Our interpretation is supported by idealised numerical simulations of stadial periods and parallel $CO_{2,atm}$ change forced by freshwater fluxes to the North Atlantic (see crosses in Fig. 6c and review of Gottschalk et al., 2019). Although these simulations have slightly different experimental designs, background conditions and forcing functions, the simulated $CO_{2,atm}$ change at the end of stadials is broadly consistent with our observations (Fig. 6c; e.g., Schmittner and Galbraith, 2008; Bouttes et al., 2012). Moreover, the $CO_{2,atm}$ change in these simulations is largely driven by ocean carbon release (albeit from different ocean reservoirs) with compensatory effects from carbon inventory changes in the terrestrial biosphere (e.g., Marchal et al., 1998; Schmittner and Galbraith, 2008; Bouttes et al., 2012; Menviel et al., 2014). This emphasises that the observed millennial adjustment timescale of $CO_{2,atm(-PRED)}$ in Fig. 6c is consistent with an influence from deep-ocean ventilation (e.g., Schmittner and Galbraith, 2008).

However, during short stadials, rapid changes in the terrestrial biosphere such as the decline of boreal forests and/or the expansion of southern-hemisphere land vegetation may dominate the atmospheric carbon inventory (e.g., Köhler et al., 2005; Menviel et al., 2008; Bozbiyik et al., 2011; Bouttes et al., 2012). This may also be influenced by fast upper-ocean carbon release through SHW strengthening (Menviel et al., 2018) or rapid sea ice changes (Rae et al., 2018). Numerical simulations show that modelled $CO_{2,atm}$ change during short stadials (<700 yr) mostly range between ~−7 and +7 ppm depending on the interplay between oceanic versus terrestrial processes (Fig. 6c; Gottschalk et al., 2019), while $CO_{2,atm}$ change observed in the Siple Dome ice core was suggested to be negligibly small during those intervals (Ahn and Brook, 2014). Two different processes driving centennial- to millennial-scale $CO_{2,atm}$ change during stadials may thus be identified: the first is connected with a fast responding carbon reservoir such as the upper ocean

Please cite this article as: Gottschalk, J et al., Southern Ocean link between changes in atmospheric CO_2 levels and northern-hemisphere climate anomalies during the last two glacial periods, Quaternary Science Reviews, https://doi.org/10.1016/j.quascirev.2019.106067

and/or the terrestrial biosphere; the second is driven by slow and gradual adjustments in the deep ocean (i.e., deep-ocean ventilation and -overturning).

The relationship between the duration of an AMOC perturbation (i.e., stadial) and deep South Atlantic respired carbon/oxygen- and $CO_{2,atm(-PRED)}$ change is similar during MIS 3 and MIS 6 (Fig. 6b and c). The rate of respired carbon loss from the deep (southern, high-latitude) ocean during northern-hemisphere stadials was hence not discernibly different during MIS 3 and 6. This observation is important in light of proposed differences in the oceanic settings during the last two glacial periods: Margari et al. (2010) suggested that the AMOC was overall weaker during MIS 6, as shown by different baseline epibenthic $\delta^{13}C$ values at the Iberian margin during MIS 3 and MIS 6 (Fig. 7e). A generally weaker AMOC during MIS 6 may have resulted from a reduced density of northern-sourced water masses owing to a stronger hydrological cycle in the mid-latitude North Atlantic (Margari et al., 2010). Furthermore, the change in Antarctic temperature and in SST at our core site (Fig. 7b) is much smaller in MIS 6 for a given stadial duration than in MIS 3 (Margari et al., 2010), and may suggest weaker AMOC perturbations and less intense Southern Ocean upwelling and deep-ocean ventilation during MIS 6. Additionally, increased IRD abundances at our study site during North Atlantic stadials in MIS 6 imply stronger ice wasting and/or -export during periods of Antarctic warming, when compared to MIS 3, which could have had implications for the density structure of the Southern Ocean surface, and hence ocean-atmosphere CO_2 fluxes during MIS 3 and MIS 6. However, despite these dynamic and hydrographic differences, we do not resolve any systematic differences in the rate and magnitude of respired carbon loss from the deep sub-Antarctic Atlantic and associated $CO_{2,atm(-PRED)}$ change during the last two glacial periods. Although uncertainties of our estimates are quite large, in particular with respect to $CO_{2,atm-PRED}$ change during MIS 6, this suggests that the rate of Southern Ocean CO_2 outgassing is similar during northern-hemisphere stadials of both glacial periods (Fig. 7). However, the degree to which compensatory effects in MIS 6, such as when a larger respired deep-ocean carbon pool and weaker AMOC/Southern Ocean perturbations are combined, cause a similar $CO_{2,atm}$ rate of change as in MIS 3 remains unconstrained. High-resolution ice core $CO_{2,atm}$ measurements in MIS 6 are needed to verify these findings.

5.2.3. Comparison with equilibrium climate model simulations

Numerical simulations forced by freshwater hosing in the North Atlantic produce a weakened AMOC (i.e., stadial conditions) that is qualitatively consistent with our observations (Gottschalk et al., 2019). A subset of these freshwater hosing experiments find that changes in Southern Ocean vertical mixing and -carbon release during AMOC perturbations are the main driver of simulated ocean carbon loss and increase in $CO_{2,atm}$ at that time (Schmittner et al., 2007; Schmittner and Galbraith, 2008; Schmittner and Lund, 2015). This is supported by Menviel et al. (2008, 2014, 2015a, 2015b, 2018), who highlight that an agreement of simulated and observed $CO_{2,atm}$ changes during stadial periods can only be achieved through an increase in AABW formation and Southern Ocean convection. Our proxy data support these model findings and highlight the operation of a bipolar seesaw in deep ocean convection between the northern and southern hemispheres ("ventilation seesaw") during the last two glacial periods, which extends the findings of Skinner et al. (2014) to the last two glacial periods.

Intensifications and/or poleward shifts of the SHW were also suggested to occur in parallel with AMOC perturbations and to increase ocean ventilation and ocean-to-atmosphere CO_2 fluxes, with implications for $CO_{2,atm}$ (Anderson et al., 2009; Lee et al., 2011; Jaccard et al., 2016; Chiang et al., 2018; Pedro et al., 2018). This can be assessed based on numerical simulations that are forced by changes in the SHW, taking advantage of the recent compilation of Gottschalk et al. (2019).

Model simulations forced by increases in the SHW wind intensity show a $CO_{2,atm}$ rise owing to enhanced Ekman pumping and ocean carbon loss primarily, but not exclusively, from intermediate depths (~500–2000 m) (Gottschalk et al., 2019). These simulations would be consistent with our observations, if ocean carbon loss from the deep South Atlantic was also significantly affected. With the exception of model simulations of Völker and Köhler (2013), numerical models forced by southward shifts of the SHW show a reduction in the surface outcrop area of deep water masses in the Southern Ocean, which decreases the simulated ocean-atmosphere CO_2 flux, and therefore lowers $CO_{2,atm}$ levels (Gottschalk et al., 2019). These simulations predict increased deep-ocean carbon storage in the South Atlantic during North Atlantic stadials, and would hence contradict our findings.

In summary, while equilibrium model simulations support our proxy data-based interpretation of an oceanic driver of millennial-scale $CO_{2,atm}$ variations, the relative contributions from Southern Ocean vertical mixing and/or wind-driven Ekman pumping, both potentially representing a Southern Ocean response to North Atlantic climate anomalies (e.g., Anderson and Carr, 2010), cannot be unraveled based on our proxy data.

5.2.4. Comparison with transient model simulations

To gain more insights into the possible drivers of observed deep South Atlantic respired carbon changes, we compare our proxy data with recent transient model simulations of the last early deglaciation (Heinrich (H) stadial 1) performed with LOVECLIM, an Earth system model of intermediate complexity (Menviel et al., 2018). These simulations test the influence of a shutdown of the AMOC on $CO_{2,atm}$ levels (Fig. 8; Menviel et al., 2018) through freshwater supply to the North Atlantic (0.04–0.07 Sv, 19 to 16.2 kyr) and to the Southern Ocean (0.1 Sv, 19 to 15 kyr), as well as a 20%-weakening of the SHW (simulation 'LH1'). They also analyse the influence of a surface buoyancy-driven and wind-driven increase in Southern Ocean convection stimulated through prescribing salt fluxes in the Southern Ocean (simulation 'LH1-SO'; −1.5 Sv, 18-15 kyr) or intensifications of the SHW wind stress (simulation 'LH1-SHW'; 20%-increase, 18.3 to 15 kyr). Simulation 'LH1-SO-SHW' combines changes in surface buoyancy and winds, and applies both a SHW intensification and negative Southern Ocean freshwater fluxes.

We derive depth-varying $[O_2]$ and DIC anomalies for H1 for the South Atlantic (60°W-20°E, 40–70°S) and the Southern Ocean (40–70°S) for each of these simulations by referencing the simulated water column profiles from model year 15 kyr to background levels at model year 18 kyr (Fig. 8a and b), and compare transient changes with our South Atlantic proxy data (Fig. 8c). The simulations show a 3 kyr-period of AMOC suppression, which is at the upper end of stadial durations considered here (Fig. 6c). Although these simulations apply transient changes in the orbital parameters and northern-hemisphere ice sheet evolution that are appropriate for H1, we assume that the model results provide insights into the dynamics during other earlier North Atlantic stadial periods.

Simulations LH1-SO and LH1-SO-SHW are characterised by increased AABW formation, and the upwelling of CO_2-rich Circumpolar Deep water, which leads to a carbon loss from the deep ocean, both from the Southern and Pacific Oceans, and a simulated $CO_{2,atm}$ rise of 10–20 ppm (see Fig. 3 in Menviel et al., 2018). These findings are qualitatively consistent with our interpretation of the proxy data, although there are offsets in absolute bottom water $[O_2]$ anomalies between the model and proxy data (Fig. 8a and b). However, transient changes in simulated bottom

Please cite this article as: Gottschalk, J et al., Southern Ocean link between changes in atmospheric CO_2 levels and northern-hemisphere climate anomalies during the last two glacial periods, Quaternary Science Reviews, https://doi.org/10.1016/j.quascirev.2019.106067

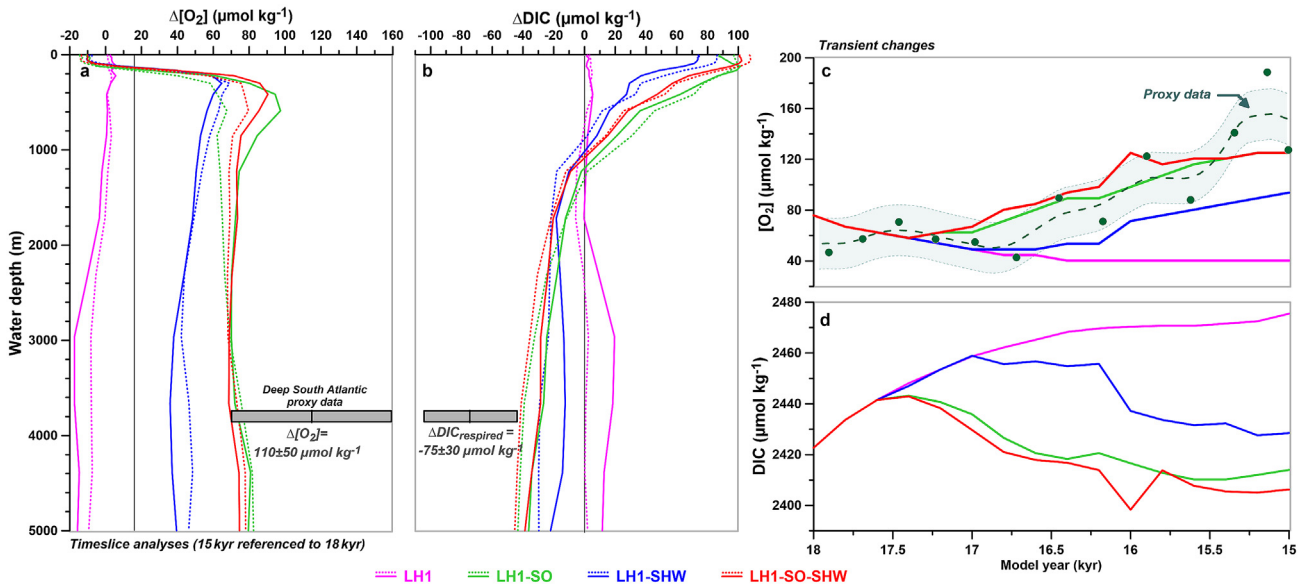

Fig. 8. Geochemical fingerprints of different forcings of millennial-scale $CO_{2,atm}$ variations in transient climate model simulations performed with LOVECLIM (Menviel et al., 2018**).** Water column profiles of (a) [O_2] and (b) DIC anomalies averaged over the South Atlantic (solid lines; 60°W-20°E, 40–70°S) and the Southern Ocean (stippled lines; 40–70°S). Simulated transient changes of (c) [O_2] and (d) DIC anomalies at our South Atlantic core site (lines) compared to reconstructed bottom water [O_2] in core MD07-3076Q (dark green, cf. Fig. 4). The depth profiles show anomalies at model year 15 kyr referenced to background levels at model year 18 kyr, and represent a Heinrich (H) stadial 1 anomaly. The simulations apply transient changes in orbital parameters and in northern-hemisphere ice sheet characteristics for H1, and force a shutdown of the AMOC through time-varying freshwater supply in the North Atlantic (simulation 'LH1'). They additionally stimulate increased Southern Ocean convection through prescribed changes in the surface buoyancy fluxes in the Southern Ocean without (simulation 'LH1-SO') or with intensification of the southern-hemisphere westerly (SHW) wind stress (simulation 'LH1-SO-SHW'), or in fact with stronger SHW winds only (simulation 'LH1-SHW'). Grey bars indicate mean changes and 1σ-uncertainties of bottom water [O_2] and respired DIC levels at depth during millennial-scale rises in $CO_{2,atm}$ during MIS 3 derived from proxy reconstructions in core MD07-3076Q (Fig. 4; Gottschalk et al., 2016a).

water [O_2] in the South Atlantic closely resemble our smoothed proxy record (Fig. 8c), and are hence consistent with a loss of (respired) carbon from the South Atlantic (Fig. 8d).

In simulation LH1, Southern Ocean convection is suppressed due to parallel freshwater hosing in the Southern Ocean and weakened SHW winds (Menviel et al., 2018). This leads to little change in simulated $CO_{2,atm}$ levels owing to a balance between increased ventilation and release of carbon from North Pacific intermediate depths and increased Atlantic carbon storage (Menviel et al., 2018). This is at odds with our proxy data (Fig. 8) and observed $CO_{2,atm}$ change during long stadials (Fig. 6c). In the SHW-driven simulation (LH1-SHW), $CO_{2,atm}$ increases on a centennial timescale, because upper Southern Ocean convection increases and respired carbon is rapidly lost primarily from the upper and intermediate ocean (Menviel et al., 2018). Its impact on simulated deep-ocean [O_2] and DIC is however minimal compared to what our proxy data suggest (Fig. 8). Although our deep-ocean proxy data cannot rule out a SHW-driven mechanism, they highlight that changes in the SHW geometry have likely not operated alone to change $CO_{2,atm}$.

Overall, simulated geochemical anomalies in the South Atlantic and the Southern Ocean strongly resemble each other (Fig. 8), which suggests that our deep South Atlantic core site may be representative of a wider region of the Southern Ocean. Our proxy data comparison with the transient simulations of Menviel et al. (2018) corroborates our proxy interpretations of a role of Southern Ocean vertical mixing in changes of deep-ocean respired carbon storage, and hence millennial-scale $CO_{2,atm}$ variations, during North Atlantic stadials of the last two glacial periods.

6. Conclusion

We extend existing high-resolution proxy reconstructions of deep South Atlantic bottom water oxygen changes, and by inference variations in respired carbon content, from the last glacial period to MIS 6. Mainly based on sedimentary redox-proxies, we show that during both glacial periods respired carbon levels in the deep South Atlantic changed in parallel with millennial-scale $CO_{2,atm}$ variations. Our observations support earlier findings of a contribution of increased Southern Ocean convection and ocean-to-atmosphere CO_2 fluxes in the Southern Ocean to increases in millennial-scale $CO_{2,atm}$ concentrations.

Our foraminiferal U/Mn data suggest that respired carbon storage was overall slightly larger during MIS 6 than during MIS 3 in the deep South Atlantic, possibly due to more expansive southern-sourced water masses and a shallower AMOC cell, more expansive Antarctic sea ice cover and overall colder conditions in the Southern Ocean. These glacial differences may have accounted for overall slightly lower $CO_{2,atm}$ levels during MIS 6 than during MIS 3. Our findings suggest that glacial background climate conditions may have had an impact on glacial respired carbon storage in the deep Southern Ocean.

Our proxy data highlight that the magnitude of carbon release from the Southern Ocean was proportional to the duration of the AMOC perturbation. This suggests that the rate of $CO_{2,atm}$ change during long stadial periods (>700 yr) was broadly constant, and was primarily set by the millennial timescale for deep ocean adjustment (i.e., ocean mixing/ventilation, Southern Ocean-atmosphere CO_2 fluxes). During these stadials, the duration of the weakened AMOC may have determined the magnitude of net ocean carbon release, and hence the magnitude of $CO_{2,atm}$ rise. However, for shorter stadial periods, processes operating on centennial timescales such as adjustments of land carbon inventories, with contributions from SHW- or sea ice effects on Southern Ocean upper-ocean convection and CO_2 outgassing, may have influenced $CO_{2,atm}$ levels, because they would have overwhelmed the effects of much slower deep-ocean overturning.

Based on our proxy data and a comparison with existing numerical model simulations, we cannot discriminate between

Please cite this article as: Gottschalk, J et al., Southern Ocean link between changes in atmospheric CO_2 levels and northern-hemisphere climate anomalies during the last two glacial periods, Quaternary Science Reviews, https://doi.org/10.1016/j.quascirev.2019.106067

possible oceanic and atmospheric mechanisms driving a teleconnection between Southern Ocean carbon dynamics and North Atlantic climate anomalies, but contributions from both seem likely. A comparison with recent transient model simulations performed with LOVECLIM (Menviel et al., 2018) show the closest model-data agreement for scenarios with increased Southern Ocean convection prescribed through Southern Ocean salt fluxes at the surface, rather than SHW-only scenarios. However, whether the prescribed changes in Southern Ocean surface buoyancy forcing are realistic and how they are mechanistically linked to North Atlantic climate anomalies remains yet elusive and needs further study. A better understanding of the atmospheric and oceanic mechanisms by which interhemispheric climate variability affect the Southern Ocean carbon cycle and $CO_{2,atm}$ (for instance through buoyancy-driven Southern Ocean vertical mixing, SHW-driven Ekman pumping, and/or Antarctic sea ice extent) may ultimately emerge from tandem reconstructions of respired carbon reconstruction at intermediate and deep sites throughout the global ocean, and through comparison with existing and evolving climate model simulations.

Acknowledgements

This study was supported by the Gates Cambridge Trust, the German Research Foundation (through grant GO 2294/2-1 to J.G.), the Royal Society, NERC grant NE/J010545/1, the Cambridge Newton Trust (L.C.S.), the Swiss National Science Foundation (grants PP00P2_144811 and 200021_163003 to S.L.J.), the Australian Research Council (grant DE150100107 and FT180100606 to L.M.), and the European Research Concil (grant 339108 to C.W.). We thank Jinhwa Shin and Jérôme Chappellaz (Institut des Géosciences de l'Environnement, Grenoble, France) for fruitful discussions of $CO_{2,atm}$ variability in MIS 6, and Sophie Hines and Jerry McManus for sharing views on inter-hemispheric climate variability. Allison Jacobel and Babette Hoogakker are thanked for insightful discussions of the $\Delta\delta^{13}C$-[O_2] proxy. We are also grateful to Linda Booth, Adam Scrivner, Tim Setzkorn and Salima Souanef-Ureta for laboratory support, and sincerely thank three anonymous reviewers for their thoughtful and constructive feedback. Age models for the study cores and data presented in this study are available from the PANGAEA website (https://doi.pangaea.de/10.1594/PANGAEA.898193).

Appendix A. Supplementary data

Supplementary data to this article can be found online at https://doi.org/10.1016/j.quascirev.2019.106067.

References

Adkins, J.F., 2013. The role of deep ocean circulation in setting glacial climates. Paleoceanography 28, 539–561. https://doi.org/10.1002/palo.20046.

Ahn, J., Brook, E.J., 2014. Siple Dome ice reveals two modes of millennial CO_2 change during the last ice age. Nat. Commun. 5 (3723) https://doi.org/10.1038/ncomms4723.

Anderson, R.F., Ali, S., Bradtmiller, L.I., Nielsen, S.H.H., Fleisher, M.Q., Anderson, B.E., Burckle, L.H., 2009. Wind-driven upwelling in the Southern Ocean and the deglacial rise in atmospheric CO_2. Science 323, 1443–1448. https://doi.org/10.1126/science.1167441.

Anderson, R.F., Barker, S., Fleisher, M., Gersonde, R., Goldstein, S.L., Kuhn, G., Mortyn, P.G., Pahnke, K., Sachs, J.P., 2014. Biological response to millennial variability of dust supply in the Subantarctic South Atlantic Ocean. Philos. Trans. R. Soc. 372 (20130054) https://doi.org/10.1098/rsta.2013.0054.

Anderson, R.F., Carr, M.-E., 2010. Uncorking the Southern Ocean's vintage CO_2. Science 328, 1117–1118. https://doi.org/10.1126/science.1190765.

Anderson, R.F., Fleisher, M.Q., LeHuray, A.P., 1989. Concentration, oxidation state, and particulate flux of uranium in the Black Sea. Geochem. Cosmochim. Acta 53, 2215–2224. https://doi.org/10.1016/0016-7037(89)90345-1.

Anderson, R.F., Sachs, J.P., Fleisher, M.Q., Allen, K.A., Yu, J., Koutavas, A., Jaccard, S.L., 2019. Deep-sea oxygen depletion and ocean carbon sequestration during the last ice age global biogeochemical cycles. Glob. Biogeochem. Cycles 33, 1–17. https://doi.org/10.1029/2018GB006049.

Bacastow, B., 1996. The effect of temperature change of the warm surface waters of the oceans on atmospheric CO_2. Global Biogeochem. Cycles 10, 319–333. https://doi.org/10.1029/96GB00039.

Barker, S., Diz, P., 2014. Timing of the descent into the last ice age determined by the bipolar seesaw. Paleoceanography 29, 489–507. https://doi.org/10.1002/2014PA002623.

Barker, S., Elderfield, H., 2002. Foraminiferal calcification response to glacial-interglacial changes in atmospheric CO_2. Science 297, 833–836. https://doi.org/10.1126/science.1072815.

Barker, S., Greaves, M., Elderfield, H., 2003. A study of cleaning procedures used for foraminiferal Mg/Ca paleothermometry. Geochem. Geophys. Geosyst. 4 (8407) https://doi.org/10.1029/2003GC000559.

Barker, S., Knorr, G., Edwards, R.L., Parrenin, F., Putnam, A.E., Skinner, L.C., Wolff, E., Ziegler, M., 2011. 800,000 Years of abrupt climate variability. Science 334, 347–351. https://doi.org/10.1126/science.1203580.

Barnes, C.E., Cochran, J.K., 1990. Uranium removal in oceanic sediments and the oceanic U balance. Earth Planet. Sci. Lett. 97, 94–101. https://doi.org/10.1016/0012-821X(90)90101-3.

Basak, C., Fröllje, H., Lamy, F., Gersonde, R., Benz, V., Anderson, R.F., Molina-kescher, M., Pahnke, K., 2018. Breakup of last glacial deep stratification in the South Pacific. Science 359, 900–904. https://doi.org/10.1126/science.aao2473.

Bazin, L., Landais, A., Lemieux-Dudon, B., Toyé Mahamadou Kele, H., Veres, D., Parrenin, F., Martinerie, P., Ritz, C., Capron, E., Lipenkov, V., Loutre, M.-F., Raynaud, D., Vinther, B., Svensson, A., Rasmussen, S.O., Severi, M., Blunier, T., Leuenberger, M., Fischer, H., Masson-Delmotte, V., Chappellaz, J., Wolff, E., 2013. An optimized multi-proxy, multi-site Antarctic ice and gas orbital chronology (AICC2012): 120-800 ka. Clim. Past 9, 1715–1721. https://doi.org/10.5194/cp-9-1715-2013.

Benz, V., Esper, O., Gersonde, R., Lamy, F., Tiedemann, R., 2016. Last Glacial Maximum sea surface temperature and sea-ice extent in the Pacific sector of the Southern Ocean. Quat. Sci. Rev. 146, 216–237. https://doi.org/10.1016/j.quascirev.2016.06.006.

Bereiter, B., Eggleston, S., Schmitt, J., Nehrbass-Ahles, C., Stocker, T.F., Fischer, H., Kipfstuhl, S., Chappellaz, J., 2015. Revision of the EPICA Dome C CO_2 record from 800 to 600 kyr before present. Geophys. Res. Lett. 42, 542–549. https://doi.org/10.1002/2014GL061957.

Bereiter, B., Lüthi, D., Siegrist, M., Schüpbach, S., Stocker, T.F., Fischer, H., 2012. Mode change of millennial CO_2 variability during the last glacial cycle associated with a bipolar marine carbon seesaw. Proc. Natl. Acad. Sci. 109, 9755–9760. https://doi.org/10.1073/pnas.1204069109.

Boiteau, R., Greaves, M., Elderfield, H., 2012. Authigenic uranium in foraminiferal coatings: a proxy for ocean redox chemistry. Paleoceanography 27, 1–8. https://doi.org/10.1029/2012PA002335.

Bouttes, N., Roche, D.M., Paillard, D., 2012. Systematic study of the impact of fresh water fluxes on the glacial carbon cycle. Clim. Past 8, 589–607. https://doi.org/10.5194/cp-8-589-2012.

Bozbiyik, A., Steinacher, M., Joos, F., Stocker, T.F., Menviel, L., 2011. Fingerprints of changes in the terrestrial carbon cycle in response to large reorganizations in ocean circulation. Clim. Past 7, 319–338. https://doi.org/10.5194/cp-7-319-2011.

Broecker, W.S., Lynch-Stieglitz, J., Archer, D., Hofmann, M., Maier-Reimer, E., Marchal, O., Stocker, T.F., Gruber, N., 1999. How strong is the Harvardton-Bear constraint? Glob. Biogeochem. Cycles 13, 817–820. https://doi.org/10.1029/1999GB900050.

Broecker, W.S., Yu, J., Putnam, A.E., 2015. Two contributors to the glacial CO_2 decline. Earth Planet. Sci. Lett. 429, 191–196. https://doi.org/10.1016/j.epsl.2015.07.019.

Buizert, C., Sigl, M., Severi, M., Markle, B.R., Wettstein, J.J., McConnell, J.R., Pedro, J.B., Sodemann, H., Goto-Azuma, K., Kawamura, K., Fujita, S., Motoyama, H., Hirabayashi, M., Uemura, R., Stenni, B., Parrenin, F., He, F., Fudge, T.J., Steig, E.J., 2018. Abrupt ice-age shifts in southern westerly winds and Antarctic climate forced from the north. Nature 563, 681–685. https://doi.org/10.1038/s41586-018-0727-5.

Calvert, S.E., Pedersen, T.F., 1996. Sedimentary geochemistry of manganese: implications for the environment of formation of manganiferous black shale. Econ. Geol. 91, 36–47. https://doi.org/10.2113/gsecongeo.91.1.36.

Cartapanis, O., Galbraith, E.D., Bianchi, D., Jaccard, S.L., 2018. Carbon burial in deep-sea sediment and implications for oceanic inventories of carbon and alkalinity over the last glacial cycle. Clim. Past 14, 1819–1850. https://doi.org/10.5194/cp-2018-49.

Carter, L., McCave, I.N., Williams, M.J.M., 2009. Circulation and water masses of the Southern Ocean: a review. Dev. Earth Environ. Sci. 8, 85–114. https://doi.org/10.1016/S1571-9197(08)00004-9.

Chalk, T.B., Foster, G.L., Wilson, P.A., 2019. Dynamic storage of glacial CO_2 in the Atlantic Ocean revealed by boron [CO_3^{2-}] and pH records. Earth Planet. Sci. Lett. 510, 1–11. https://doi.org/10.1016/j.epsl.2018.12.022.

Channell, J.E.T., Vázquez Riveiros, N., Gottschalk, J., Waelbroeck, C., Skinner, L.C., 2017. Age and duration of Laschamp and Iceland basin geomagnetic excursions in the south Atlantic Ocean. Quat. Sci. Rev. 167, 1–13. https://doi.org/10.1016/j.quascirev.2017.04.020.

Charles, C.D., Pahnke, K., Zahn, R., Mortyn, P.G., Ninnemann, U., Hodell, D.A., 2010. Millennial scale evolution of the Southern Ocean chemical divide. Quat. Sci. Rev. 29, 399–409. https://doi.org/10.1016/j.quascirev.2009.09.021.

Chase, Z., Kohfeld, K.E., Matsumoto, K., 2015. Controls on biogenic silica burial in the

Southern Ocean. Glob. Biogeochem. Cycles 29, 1–18. https://doi.org/10.1002/2015GB005186.
Chen, P., Yu, J., Jin, Z., 2017. An evaluation of benthic foraminiferal U/Ca and U/Mn proxies for deep ocean conditions. Geochem. Geophys. Geosyst. 18, 617–630. https://doi.org/10.1002/2016GC006730.
Chiang, J.C.H., Tokos, K.S., Lee, S.Y., Matsumoto, K., 2018. Contrasting impacts of the south Pacific split jet and the Southern annular mode modulation on Southern Ocean circulation and biogeochemistry. Paleoceanogr. Paleoclimatol. 33, 2–20. https://doi.org/10.1002/2017PA003229.
CLIMAP project members, 1984. The last interglacial ocean. Quat. Res. 21, 123–224. https://doi.org/10.1016/0033-5894(84)90098-X.
Coplen, B., 1988. Normalization of oxygen and hydrogen isotope data. Chem. Geol. 12, 293–297. https://doi.org/10.1016/0168-9622(88)90042-5.
Corliss, B.H., Emerson, S., 1990. Distribution of rose bengal stained deep-sea benthic foraminifera from the Nova Scotian continental margin and Gulf of Maine. Deep Sea Res. Part A. Oceanogr. Res. Pap. 37, 381–400. https://doi.org/10.1016/0198-0149(90)90015-N.
Dansgaard, W., Johnsen, S.J., Clausen, H.B., Dahl-Jensen, D., Gundestrup, N.S., Hammer, C.U., Hvidberg, C.S., Steffensen, J.P., Sveinbjörnsdottir, A.E., Jouzel, J., Bond, G.C., 1993. Evidence for general instability of past climate from a 250-kyr ice-core record. Nature 364, 218–220. https://doi.org/10.1038/364218a0.
de Abreu, L., Shackleton, N.J., Schönfeld, J., Hall, M., Chapman, M., 2003. Millennial-scale oceanic climate variability off the Western Iberian margin during the last two glacial periods. Mar. Geol. 196, 1–20. https://doi.org/10.1016/S0025-3227(03)00046-X.
Denton, G.H., Anderson, R.F., Toggweiler, J.R., Edwards, R.L., Schaefer, J.M., Putnam, A.E., 2010. The last glacial termination. Science 328, 1652–1656. https://doi.org/10.1126/science.1184119.
Detlef, H., Sosdian, S.M., Kender, S., Lear, C.H., Hall, I.R., 2020. Multi-elemental composition of authigenic carbonates in benthic foraminifera from the eastern Bering Sea continental margin (International Ocean Discovery Program Site U1343). Geochim. Cosmochim. Acta 268, 1–21. https://doi.org/10.1016/j.gca.2019.09.025.
Eggleston, S., Schmitt, J., Bereiter, B., Schneider, R., Fischer, H., 2016. Evolution of the stable carbon isotope composition of atmospheric CO_2 over the last glacial cycle. Paleoceanography 31, 434–452. https://doi.org/10.1002/2015PA002874.
EPICA Community Members, 2006. One-to-one coupling of glacial climate variability in Greenland and Antarctica. Nature 444, 195–198. https://doi.org/10.1038/nature05301.
Eppley, R.W., 1972. Temperature and phytoplankton growth in the sea. Fish. Bull. 70, 1063–1085.
Ferrari, R., Jansen, M.F., Adkins, J.F., Burke, A., Stewart, A.L., Thompson, A.F., 2014. Antarctic sea ice control on ocean circulation in present and glacial climates. Proc. Natl. Acad. Sci. 111, 8753–8758. https://doi.org/10.1073/pnas.1323922111.
Fischer, H., Schmitt, J., Lüthi, D., Stocker, T.F., Tschumi, T., Parekh, P., Joos, F., Köhler, P., Barbante, C., Le Floch, M., Raynaud, D., Wolff, E., 2010. The role of Southern Ocean processes in orbital and millennial CO_2 variations- a synthesis. Quat. Sci. Rev. 29, 193–205. https://doi.org/10.1016/j.quascirev.2009.06.007.
François, R., Altabet, M.A., Yu, E.F., Sigman, D.M., Bacon, M.P., Frank, M., Bohrmann, G., Bareille, G., Labeyrie, L.D., 1997. Contribution of Southern Ocean surface-water stratification to low atmospheric CO_2 concentrations during the last glacial period. Nature 389, 929–936. https://doi.org/10.1038/40073.
Froelich, P.N., Klinkhammer, G.P., Bender, M.L., Luedtke, N.A., Heath, G.R., Cullen, D., Dauphin, P., Hammond, D., Hartman, B., 1979. Early oxidation of organic matter in pelagic sediments of the eastern equatorial Atlantic: suboxic diagenesis. Geochem. Cosmochim. Acta 43, 1075–1090. https://doi.org/10.1016/0016-7037(79)90095-4.
Galbraith, E.D., Jaccard, S.L., 2015. Deglacial weakening of the oceanic soft tissue pump: global constraints from sedimentary nitrogen isotopes and oxygenation proxies. Quat. Sci. Rev. 109, 38–48. https://doi.org/10.1016/j.quascirev.2014.11.012.
Garcia, H.E., Locarnini, R.A., Boyer, T.P., Antonov, J.I., Baranova, O.K., Zweng, M.M., Reagan, J.R., Johnson, D.R., 2014. World Ocean Atlas 2013. In: Levitus, S., Mishonov, A.V. (Eds.), Volume 3: Dissolved Oxygen, Apparent Oxygen Utilization, and Oxygen Saturation., 75. NOAA Atlas NESDIS, p. 27.
Gebbie, G., Huybers, P., 2011. How is the ocean filled? Geophys. Res. Lett, 38 (L6604), 1–5. https://doi.org/10.1029/2011GL046769.
Gersonde, R., Abelmann, A., Brathauer, U., Becquey, S., Bianchi, C., Cortese, G., Grobe, H., Kuhn, G., Niebler, H.-S., Segl, M., Sieger, M., Zielinski, U., Fütterer, D.K., 2003. Last glacial sea surface temperatures and sea-ice extent in the Southern Ocean (Atlantic-Indian sector): a multiproxy approach. Paleoceanography 18 (3), 1–18. https://doi.org/10.1029/2002PA000809.
Geslin, E., Heinz, P., Jorissen, F., Hemleben, C., 2004. Migratory responses of deep-sea benthic foraminifera to variable oxygen conditions: laboratory investigations. Mar. Micropaleontol. 53, 227–243. https://doi.org/10.1016/j.marmicro.2004.05.010.
Glock, N., Roy, A.S., Romero, D., Wein, T., Weissenbach, J., Revsbech, N.P., Høgslund, S., Clemens, D., Sommer, S., Dagan, T., 2019. Metabolic preference of nitrate over oxygen as an electron acceptor in foraminifera from the Peruvian oxygen minimum zone. Proc. Natl. Acad. Sci. 116, 2860–2865. https://doi.org/10.1073/pnas.1813887116.
Gottschalk, J., Battaglia, G., Fischer, H., Frölicher, T., Jaccard, S.L., Jeltsch-Thömmes, A., Joos, F., Köhler, P., Meissner, K.J., Menviel, L., Nehrbass-Ahles, C., Schmitt, J., Schmittner, A., Skinner, L.C., Stocker, T.F., 2019. Mechanisms of millennial-scale atmospheric CO_2 change in numerical model simulations. Quat. Sci. Rev. 220, 30–74. https://doi.org/10.1016/j.quascirev.2019.05.013.
Gottschalk, J., Hodell, D.A., Skinner, L.C., Crowhurst, S.J., Jaccard, S.L., Charles, C.D., 2018. Implications of past carbonate preservation events in the deep Southeast Atlantic (Cape Basin) for Atlantic overturning dynamics and the global carbon cycle. Paleoceanogr. Paleoclimatol. 33, 1–21. https://doi.org/10.1029/2018PA003353.
Gottschalk, J., Vazquez Riveiros, N., Waelbroeck, C., Skinner, L.C., Michel, E., Duplessy, J.-C., Hodell, D., Mackensen, A., 2016b. Carbon isotope offsets between species of the genus *Cibicides (Cibicidoides)* in the glacial sub-Antarctic Atlantic Ocean. Paleoceanography 31, 1583–1602. https://doi.org/10.1002/2016PA003029.
Gottschalk, J., Skinner, L.C., Lippold, J., Vogel, H., Frank, N., Jaccard, S.L., Waelbroeck, C., 2016a. Biological and physical controls in the Southern Ocean on past millennial-scale atmospheric CO_2 changes. Nat. Commun. 7, 1–11. https://doi.org/10.1038/ncomms11539.
Gottschalk, J., Skinner, L.C., Misra, S., Waelbroeck, C., Menviel, L., Timmermann, A., 2015a. Abrupt changes in the southern extent of North Atlantic Deep Water during Dansgaard-Oeschger events. Nat. Geosci. 8, 950–955. https://doi.org/10.1038/ngeo2558.
Gottschalk, J., Skinner, L.C., Waelbroeck, C., 2015b. Contribution of seasonal sub-Antarctic surface water variability to millennial-scale changes in atmospheric CO_2 over the last deglaciation and Marine Isotope Stage 3. Earth Planet. Sci. Lett. 411, 87–99. https://doi.org/10.1016/j.epsl.2014.11.051.
Haddam, N.A., Michel, E., Siani, G., Cortese, G., Bostock, H.C., Duprat, J.M., Isguder, G., 2016. Improving past sea surface temperature reconstructions from the Southern Hemisphere oceans using planktonic foraminiferal census data. Paleoceanography 31, 822–837. https://doi.org/10.1002/2016PA002946.
Hain, M.P., Sigman, D.M., Haug, G.H., 2010. Carbon dioxide effects of Antarctic stratification, North Atlantic Intermediate Water formation, and subantarctic nutrient drawdown during the last ice age: diagnosis and synthesis in a geochemical box model. Global Biogeochem. Cycles 24 (GB4023), 1–19. https://doi.org/10.1029/2010GB003790.
Hasenfratz, A.P., Martínez-García, A., Jaccard, S.L., Vance, D., Wälle, M., Greaves, M., Haug, G.H., 2016. Determination of the Mg/Mn ratio in foraminiferal coatings: an approach to correct Mg/Ca temperatures for Mn-rich contaminant phases. Earth Planet. Sci. Lett. 457, 335–347. https://doi.org/10.1016/j.epsl.2016.10.004.
Haslett, J., Parnell, A., 2008. A simple monotone process with application to radiocarbon-dated depth chronologies. J. R. Stat. Soc. 57, 399–418. https://doi.org/10.1111/j.1467-9876.2008.00623.x.
Hemming, S.R., 2010. Heinrich events: massive late Pleistocene detritus layers of the North Atlantic and their global climate imprint. Rev. Geophys. 42 (RG1005), 1–43. https://doi.org/10.1029/2003RG000128.
Henry, L.G., McManus, J.F., Curry, W.B., Roberts, N.L., Piotrowski, A.M., Keigwin, L.D., 2016. North Atlantic ocean circulation and abrupt climate change during the last glaciation. Science 353, 470–474. https://doi.org/10.1126/science.aaf5529.
Hoogakker, B.A.A., Elderfield, H., Schmiedl, G., McCave, I.N., Rickaby, R.E.M., 2015. Glacial-interglacial changes in bottom-water oxygen content on the Portuguese margin. Nat. Geosci. 8, 40–43. https://doi.org/10.1038/ngeo2317.
Huybers, P., Langmuir, C., 2009. Feedback between deglaciation, volcanism, and atmospheric CO_2. Earth Planet. Sci. Lett. 286, 479–491. https://doi.org/10.1016/j.epsl.2009.07.014.
Ito, T., Follows, M.J., 2005. Preformed phosphate, soft tissue pump and atmospheric CO_2. J. Mar. Res. 63, 813–839. https://doi.org/10.1357/0022240054663231.
Jaccard, S.L., Galbraith, E.D., 2012. Large climate-driven changes of oceanic oxygen concentrations during the last deglaciation. Nat. Geosci. 5, 151–156. https://doi.org/10.1038/ngeo1352.
Jaccard, S.L., Galbraith, E.D., Frölicher, T.L., Gruber, N., 2014. Ocean (de)oxygenation across the last deglaciation: insights for the future. Oceanography 27, 26–35. https://doi.org/10.5670/oceanog.2014.05.
Jaccard, S.L., Galbraith, E.D., Martínez-Garcia, A., Anderson, R.F., 2016. Covariation of abyssal Southern Ocean oxygenation and pCO_2 throughout the last ice age. Nature 530, 207–210. https://doi.org/10.1038/nature16514.
Jaccard, S.L., Galbraith, E.D., Sigman, D.M., Haug, G.H., François, R., Pedersen, T.F., Dulski, P., Thierstein, H.R., 2009. Subarctic Pacific evidence for a glacial deepening of the oceanic respired carbon pool. Earth Planet. Sci. Lett. 277, 156–165. https://doi.org/10.1016/j.epsl.2008.10.017.
Jaccard, S.L., Hayes, C.T., Martínez-García, A., Hodell, D.A., Anderson, R.F., Sigman, D.M., Haug, G.H., 2013. Two modes of change in Southern Ocean productivity over the past million years. Science 339, 1419–1423. https://doi.org/10.1126/science.1227545.
Jacobel, A., Anderson, R., Jaccard, S., McManus, J., Pavia, F., Winckler, G., 2019. Deep Pacific storage of respired carbon during the Last Ice Age: perspectives from bottom water oxygen reconstructions. Quat. Sci. Rev. https://doi.org/10.1016/j.quascirev.2019.106065.
Jouzel, J., Masson-Delmotte, V., Cattani, O., Dreyfus, G., Falourd, S., Hoffmann, G., Minster, B., Nouet, J., Barnola, J.M., Chappellaz, J., Fischer, H., Gallet, J.C., Johnsen, S., Leuenberger, M., Loulergue, L., Luethi, D., Oerter, H., Parrenin, F., Raisbeck, G., Raynaud, D., Schilt, A., Schwander, J., Selmo, E., Souchez, R., Spahni, R., Stauffer, B., Steffensen, J.P., Stenni, B., Stocker, T.F., Tison, J.L., Werner, M., Wolff, E.W., 2007. Orbital and millennial Antarctic climate variability over the past 800,000 years. Science 317, 793–796. https://doi.org/10.1126/science.1141038.
Kanfoush, S.L., Hodell, D.A., Charles, C.D., Guilderson, T.P., Mortyn, P.G., Ninnemann, U.S., 2000. Millennial-scale instability of the Antarctic ice sheet during the last glaciation. Science 288, 1815–1818. https://doi.org/10.1126/

Please cite this article as: Gottschalk, J et al., Southern Ocean link between changes in atmospheric CO_2 levels and northern-hemisphere climate anomalies during the last two glacial periods, Quaternary Science Reviews, https://doi.org/10.1016/j.quascirev.2019.106067

science.288.5472.1815.
Kasten, S., Zabel, M., Heuer, V., Hensen, C., 2003. Processes and signals of non-steady state diagenesis in deep-sea sediments and their pore waters. In: Wefer, G., Mulitza, S., Ratmeyer, V. (Eds.), The South Atlantic in the Late Quaternary: Reconstruction of Material Budgets and Current Systems. Springer-Verlag Berlin, Heidelberg New York Tokyo, pp. 431–459. https://doi.org/10.1007/978-3-642-18917-3_20.
Key, R.M., Kozyr, A., Sabine, C.L., Lee, K., Wanninkhof, R., Bullister, J.L., Feely, R.A., Millero, F.J., Mordy, C., Peng, T.-H., 2004. A global ocean carbon climatology: results from global data analysis project (GLODAP). Glob. Biogeochem. Cycles 18 (GB4031), 1–23. https://doi.org/10.1029/2004GB002247.
Klinkhammer, G.P., Palmer, M.R., 1991. Uranium in the oceans: where it goes and why. Geochem. Cosmochim. Acta 55, 1799–1806. https://doi.org/10.1016/0016-7037(91)90024-Y.
Köhler, P., Joos, F., Gerber, S., Knutti, R., 2005. Simulated changes in vegetation distribution, land carbon storage, and atmospheric CO_2 in response to a collapse of the North Atlantic thermohaline circulation. Clim. Dyn. 25, 689–708. https://doi.org/10.1007/s00382-005-0058-8.
Köhler, P., Knorr, G., Bard, E., 2014. Permafrost thawing as a possible source of abrupt carbon release at the onset of the Bølling/Allerød. Nat. Commun 5 (5520). https://doi.org/10.1038/ncomms6520.
Köhler, P., Nehrbass-Ahles, C., Schmitt, J., Stocker, T.F., Fischer, H., 2017. A 156 kyr smoothed history of the atmospheric greenhouse gases CO_2, CH_4, and N_2O and their radiative forcing. Earth Syst. Sci. Data 9, 363–387. https://doi.org/10.5194/essd-9-363-2017.
Kroopnick, P.M., 1985. The distribution of ^{13}C of Sigma CO_2 in the world oceans. Deep Sea Res. 32, 57–84. https://doi.org/10.1016/0198-0149(85)90017-2.
Kumar, N., Anderson, R.F., Mortlock, R.A., Froelich, P.N., Kubik, P., Dittrich-Hannen, B., Suter, M., 1995. Increased biological productivity and export production in the glacial Southern Ocean. Nature 378, 675–680. https://doi.org/10.1038/378675a0.
Kurahashi-Nakamura, T., Abe-Ouchi, A., Yamanaka, Y., Misumi, K., 2007. Compound effects of Antarctic sea ice on atmospheric pCO_2 change during glacial-interglacial cycle. Geophys. Res. Lett. 34, 1–5. https://doi.org/10.1029/2007GL030898.
Kwon, E.Y., Primeau, F., Sarmiento, J.L., 2009. The impact of remineralization depth on the air–sea carbon balance. Nat. Geosci. 2, 630–635. https://doi.org/10.1038/ngeo612.
Lambert, F., Bigler, M., Steffensen, J.P., Hutterli, M., Fischer, H., 2012. Centennial mineral dust variability in high-resolution ice core data from Dome C, Antarctica. Clim. Past 8, 609–623. https://doi.org/10.5194/cp-8-609-2012.
Lamy, F., Gersonde, R., Winckler, G., Esper, O., Jaeschke, A., Kuhn, G., Ullermann, J., Martinez-Garcia, A., Lambert, F., Kilian, R., 2014. Increased dust deposition in the Pacific Southern Ocean during glacial periods. Science 343, 403–407. https://doi.org/10.1126/science.1245424.
Lear, C.H., Billups, K., Rickaby, R.E.M., Diester-Haass, L., Mawbey, E.M., Sosdian, S.M., 2016. Breathing more deeply: deep ocean carbon storage during the mid-Pleistocene climate transition. Geology 44 (12), 1035–1038. https://doi.org/10.1130/G38636.1.
Lee, S.Y., Chiang, J.C.H., Matsumoto, K., Tokos, K.S., 2011. Southern Ocean wind response to North Atlantic cooling and the rise in atmospheric CO_2: modeling perspective and paleoceanographic implications. Paleoceanography 26 (1214), 1–16. https://doi.org/10.1029/2010PA002004.
Lund, D.C., Asimow, P.D., Farley, K.A., Rooney, T.O., Seeley, E., Jackson, E.W., Durham, Z.M., 2016. Enhanced East Pacific Rise hydrothermal activity during the last two glacial terminations. Science 351, 478–482. https://doi.org/10.1126/science.aad4296.
Marchal, O., Stocker, T.F., Joos, F., 1998. Impact of oceanic reorganizations on the ocean carbon cycle and atmospheric carbon dioxide content. Paleoceanography 13, 225–244. https://doi.org/10.1029/98PA00726.
Margari, V., Skinner, L.C., Tzedakis, P.C., Ganopolski, A., Vautravers, M., Shackleton, N.J., 2010. The nature of millennial-scale climate variability during the past two glacial periods. Nat. Geosci. 3, 127–131. https://doi.org/10.1038/ngeo740.
Marinov, I., Gnanadesikan, A., Toggweiler, J.R., Sarmiento, J.L., 2006. The Southern Ocean biogeochemical divide. Nature 441, 964–967. https://doi.org/10.1038/nature04883.
Martin, J.H., 1990. Glacial-interglacial CO_2 change: the iron hypothesis. Paleoceanography 5, 1–13. https://doi.org/10.1029/PA005i001p00001.
Martínez-García, A., Sigman, D.M., Ren, H., Anderson, R.F., Straub, M., Hodell, D.A., Jaccard, S.L., Eglinton, T.I., Haug, G.H., 2014. Iron fertilization of the Subantarctic Ocean during the last Ice Age. Science 343, 1347–1350. https://doi.org/10.1126/science.1246848.
Martrat, B., Grimalt, J.O., Shackleton, N.J., de Abreu, L., Hutterli, M.A., Stocker, T.F., 2007. Four climate cycles of recurring deep and surface water destabilizations on the Iberian margin. Science 317, 502–507. https://doi.org/10.1126/science.1139994.
Matsumoto, K., 2007. Biology-mediated temperature control on atmospheric pCO_2 and ocean biogeochemistry. Geophys. Res. Lett. 34 (L20605), 1–5. https://doi.org/10.1029/2007GL031301.
Matsumoto, K., Hashioka, T., Yamanaka, Y., 2007. Effect of temperature-dependent organic carbon decay on atmospheric pCO_2. J. Geophys. Res. 112, 1–9. https://doi.org/10.1029/2006JG000187.
McCorkle, D.C., Emerson, S.R., 1988. The relationship between pore water carbon isotopic composition and bottom water oxygen concentration. Geochim. Cosmochim. Acta 52, 1169–1178. https://doi.org/10.1016/0016-7037(88)90270-0.
McCorkle, D.C., Keigwin, L.D., Corliss, B.H., Emerson, S.R., 1990. The influence of microhabitats on the carbon isotopic composition of deep-sea benthic foraminifera. Paleoceanography 5, 161–185. https://doi.org/10.1029/PA005i002p00161.
McManus, J., Berelson, W.M., Klinkhammer, G.P., Hammond, D.E., Holm, C., 2005. Authigenic uranium: relationship to oxygen penetration depth and organic carbon rain. Geochem. Cosmochim. Acta 69, 95–108. https://doi.org/10.1016/j.gca.2004.06.023.
McManus, J., Berelson, W.M., Severmann, S., Poulson, R.L., Hammond, D.E., Klinkhammer, G.P., Holm, C., 2006. Molybdenum and uranium geochemistry in continental margin sediments: Paleoproxy potential. Geochem. Cosmochim. Acta 70, 4643–4662. https://doi.org/10.1016/j.gca.2006.06.1564.
Menviel, L., England, M.H., Meissner, K.J., Mouchet, A., Yu, J., 2014. Atlantic-Pacific seesaw and its role in outgassing CO_2 during Heinrich events. Paleoceanography 29, 58–70. https://doi.org/10.1002/2013PA002542.
Menviel, L., Spence, P., England, M.H., 2015a. Contribution of enhanced Antarctic Bottom Water formation to Antarctic warm events and millennial-scale atmospheric CO_2 increase. Earth Planet. Sci. Lett. 413, 37–50. https://doi.org/10.1016/j.epsl.2014.12.050.
Menviel, L., Mouchet, A., Meissner, K.J., Joos, F., England, M.H., 2015b. Impact of oceanic circulation changes on atmospheric $\delta^{13}CO_2$. Global Biogeochem. Cycles 29, 1944–1961. https://doi.org/10.1002/2015GB005207.
Menviel, L., Spence, P., Yu, J., Chamberlain, M.A., Matear, R.J., Meissner, K.J., England, M.H., 2018. Southern Hemisphere westerlies as a driver of the early deglacial atmospheric CO_2 rise. Nat. Commun. 9 (2503) https://doi.org/10.1038/s41467-018-04876-4.
Menviel, L., Timmermann, A., Mouchet, A., Timm, O., 2008. Meridional reorganizations of marine and terrestrial productivity during Heinrich events. Paleoceanography 23, PA1203. https://doi.org/10.1029/2007PA001445.
Menviel, L., Yu, J., Joos, F., Mouchet, A., Meissner, K.J., England, M.H., 2017. Poorly ventilated deep ocean at the Last Glacial Maximum inferred from carbon isotopes: a data-model comparison study. Paleoceanography 32, 2–17. https://doi.org/10.1002/2016PA003024.
Morford, J.L., Emerson, S., 1999. The geochemistry of redox sensitive trace metals in sediments. Geochim. Cosmochim. Acta 63, 1735–1750. https://doi.org/10.1016/S0016-7037(99)00126-X.
NGRIP members, 2004. High-resolution record of Northern Hemisphere climate extending into the last interglacial period. Nature 431, 147–151. https://doi.org/10.1038/nature02805.
Nielsen, S.H.H., Hodell, D.A., Kamenov, G., Guilderson, T., Perfit, M.R., 2007. Origin and significance of ice-rafted detritus in the atlantic sector of the Southern Ocean. Geochem. Geophys. Geosyst 8 (Q12005). https://doi.org/10.1029/2007GC001618.
Ödalen, M., Nycander, J., Oliver, K.I.C., Brodeau, L., Ridgwell, A., 2018. The influence of the ocean circulation state on ocean carbon storage and CO_2 drawdown potential in an Earth system model. Biogeosciences 15, 1367–1393. https://doi.org/10.5194/bg-15-1367-2018.
Orsi, A.H., Whitworth, T., Nowlin, W.D., 1995. On the meridional extent and fronts of the Antarctic Circumpolar Current. Deep Sea Res. 42, 641–673. https://doi.org/10.1016/0967-0637(95)00021-W.
Pedro, J.B., Jochum, M., Buizert, C., He, F., Barker, S., Rasmussen, S.O., 2018. Beyond the bipolar seesaw: toward a process understanding of interhemispheric coupling. Quat. Sci. Rev. 192, 27–46. https://doi.org/10.1016/j.quascirev.2018.05.005.
Pena, L.D., Cacho, I., Calvo, E., Pelejero, C., Eggins, S., Sadekov, A., 2008. Characterization of contaminant phases in foraminifera carbonates by electron microprobe mapping. Geochem. Geophys. Geosyst. 9 (Q07012), 1–12. https://doi.org/10.1029/2008GC002018.
Pena, L.D., Calvo, E., Cacho, I., Eggins, S., Pelejero, C., 2005. Identification and removal of Mn-Mg-rich contaminant phases on foraminiferal tests: implications for Mg/Ca past temperature reconstructions. Geochem. Geophys. Geosyst. 6 (Q09P02), 1–25. https://doi.org/10.1029/2005GC000930.
Petit, J.-R., Jouzel, J., Raynaud, D., Barkov, N.I., Barnola, J.-M., Basile, I., Bender, M., Chappellaz, J., Davis, M., Delaygue, G., Delmotte, M., Kotlyakov, V.M., Legrand, M., Lipenkov, V.Y., Lorius, C., Pepin, L., Ritz, C., Saltzman, E., Stievenard, M., 1999. Climate and atmospheric history of the past 420,000 years from the Vostok ice core, Antarctica. Nature 399, 429–436. https://doi.org/10.1038/20859.
Piña-Ochoa, E., Koho, K.A., Geslin, E., Risgaard-Petersen, N., 2010. Survival and life strategy of the foraminiferan *Globobulimina turgida* through nitrate storage and denitrification. Mar. Ecol. Prog. Ser. 417, 39–49. https://doi.org/10.3354/meps08805.
Policy, H.W., Johnson, H.B., Marinot, B.D., Mayeux, H.S., 1993. Increase in C3 plant water-use efficiency and biomass over glacial to present CO_2 concentrations. Nature 361 (61), 61–64. https://doi.org/10.1038/361061a0.
Primeau, F., 2005. Characterizing transport between the surface mixed layer and the ocean interior with a forward and adjoint global ocean transport model. J. Phys. Oceanogr. 35, 545–564. https://doi.org/10.1175/JPO2699.1.
Rae, J.W.B., Burke, A., Robinson, L.F., Adkins, J.F., Chen, T., Cole, C., Greenop, R., Li, T., Littley, E.F.M., Nita, D.C., Stewart, J.A., Taylor, B.J., 2018. CO_2 storage and release in the deep Southern Ocean on millennial to centennial timescales. Nature 562, 569–573. https://doi.org/10.1038/s41586-018-0614-0.
Raitzsch, M., Kuhnert, H., Hathorne, C., Groeneveld, J., Bickert, T., 2011. U/Ca in

Please cite this article as: Gottschalk, J et al., Southern Ocean link between changes in atmospheric CO_2 levels and northern-hemisphere climate anomalies during the last two glacial periods, Quaternary Science Reviews, https://doi.org/10.1016/j.quascirev.2019.106067

benthic foraminifers: a proxy for the deep-sea carbonate saturation. Geochem. Geophys. Geosyst. 12 (Q06019), 1–12. https://doi.org/10.1029/2010GC003344.
Risgaard-Petersen, N., Langezaal, A.M., Ingvardsen, S., Schmid, M.C., Jetten, M.S.M., Op Den Camp, H.J.M., Derksen, J.W.M., Piña-Ochoa, E., Eriksson, S.P., Nielsen, L.P., Revsbech, N.P., Cedhagen, T., Van Der Zwaan, G.J., 2006. Evidence for complete denitrification in a benthic foraminifer. Nature 443, 93–96. https://doi.org/10.1038/nature05070.
Roberts, J., Gottschalk, J., Skinner, L.C., Peck, V.L., Kender, S., Elderfield, H., Waelbroeck, C., Vázquez Riveiros, N., Hodell, D.A., 2015. Evolution of South Atlantic density and chemical stratification across the last deglaciation. Proc. Natl. Acad. Sci. 113, 514–519. https://doi.org/10.1073/pnas.1511252113.
Ronge, T.A., Tiedemann, R., Lamy, F., Köhler, P., Alloway, B.V., De Pol-Holz, R., Pahnke, K., Southon, J., Wacker, L., 2016. Radiocarbon constraints on the extent and evolution of the South Pacific glacial carbon pool. Nat. Commun. 7 (11487) https://doi.org/10.1038/ncomms11487.
Russell, A.D., Hönisch, B., Spero, H.J., Lea, D.W., 2004. Effects of seawater carbonate ion concentration and temperature on shell U, Mg, and Sr in cultured planktonic foraminifera. Geochem. Cosmochim. Acta 68, 4347–4361. https://doi.org/10.1016/j.gca.2004.03.013.
Sarmiento, J.L., Toggweiler, J.R., 1984. A new model for the role of the oceans in determining atmospheric pCO_2. Nature 308, 621–624. https://doi.org/10.1038/308621a0.
Schmittner, A., Brook, E.J., Ahn, J., 2007. Impact of the ocean's overturning circulation on atmospheric CO_2. In: Schmittner, A., Chiang, J.C.H., Hemming, S.R. (Eds.), Geophysical Monograph Series 173: Ocean Circulation: Mechanisms and Impacts. American Geophysical Union, Washington, DC, USA, pp. 209–246. https://doi.org/10.1029/173GM20.
Schmittner, A., Galbraith, E.D., 2008. Glacial greenhouse-gas fluctuations controlled by ocean circulation changes. Nature 456, 373–376. https://doi.org/10.1038/nature07531.
Schmittner, A., Lund, D.C., 2015. Early deglacial Atlantic overturning decline and its role in atmospheric CO_2 rise inferred from carbon isotopes ($\delta^{13}C$). Clim. Past 11, 135–152. https://doi.org/10.5194/cp-11-135-2015.
Schneider, R., Schmitt, J., Köhler, P., Joos, F., Fischer, H., 2013. A reconstruction of atmospheric carbon dioxide and its stable carbon isotopic composition from the penultimate glacial maximum to the last glacial inception. Clim. Past 9, 2507–2523. https://doi.org/10.5194/cp-9-2507-2013.
Shoenfelt, E.M., Winckler, G., Lamy, F., Anderson, R.F., Bostick, B.C., 2018. Highly bioavailable dust-borne iron delivered to the Southern Ocean during glacial periods. Proc. Natl. Acad. Sci. 115, 11180–11185. https://doi.org/10.1073/pnas.1809755115.
Sigman, D.M., Boyle, E.A., 2000. Glacial/interglacial variations in atmospheric carbon dioxide. Nature 407, 859–869. https://doi.org/10.1038/35038000.
Sigman, D.M., De Boer, A.M., Haug, G.H., 2007. Antarctic stratification, atmospheric water vapor, and Heinrich events: a hypothesis for late Pleistocene deglaciations. In: Schmittner, A., Chiang, J.C.H., Hemming, S.R. (Eds.), Geophysical Monograph Series 173: Ocean Circulation: Mechanisms and Impacts. American Geophysical Union, Washington, DC, USA, pp. 335–349. https://doi.org/10.1029/173GM21.
Sigman, D.M., Hain, M.P., Haug, G.H., 2010. The polar ocean and glacial cycles in atmospheric CO_2 concentration. Nature 466, 47–55. https://doi.org/10.1038/nature09149.
Sikes, E.L., Cook, M.S., Guilderson, T.P., 2016. Reduced deep ocean ventilation in the Southern Pacific Ocean during the last glaciation persisted into the deglaciation. Earth Planet. Sci. Lett. 438, 130–138. https://doi.org/10.1016/j.epsl.2015.12.039.
Skinner, L.C., Elderfield, H., Hall, M., 2007. Phasing of millennial climate events and Northeast Atlantic deep-water temperature change since 50 ka BP. In: Schmittner, A., Chiang, J.C.H., Hemming, S.R. (Eds.), Geophysical Monograph Series 173: Ocean Circulation: Mechanisms and Impacts. American Geophysical Union, Washington, DC, USA, pp. 197–208. https://doi.org/10.1029/173GM14.
Skinner, L.C., Fallon, S., Waelbroeck, C., Michel, E., Barker, S., 2010. Ventilation of the deep Southern Ocean and deglacial CO_2 rise. Science 328, 1147–1151. https://doi.org/10.1126/science.1183627.
Skinner, L.C., Sadekov, A., Brandon, M., Greaves, M., Plancherel, Y., de la Fuente, M., Gottschalk, J., Souanef-Ureta, S., Sevilgen, D.S., Scrivner, A.E., 2019. Rare Earth Elements in early-diagenetic foraminifer 'coatings': pore-water controls and potential palaeoceanographic applications. Geochem. Cosmochim. Acta 245, 118–132. https://doi.org/10.1016/j.gca.2018.10.027.
Skinner, L.C., Shackleton, N.J., 2005. An Atlantic lead over Pacific deep-water change across Termination I: implications for the application of the marine isotope stage stratigraphy. Quat. Sci. Rev. 24, 571–580. https://doi.org/10.1016/j.quascirev.2004.11.008.
Skinner, L.C., Waelbroeck, C., Scrivner, A.E., Fallon, S.J., 2014. Radiocarbon evidence for alternating northern and southern sources of ventilation of the deep Atlantic carbon pool during the last deglaciation. Proc. Natl. Acad. Sci. 111, 5480–5484. https://doi.org/10.1073/pnas.1400668111.
Sokolov, S., Rintoul, S.R., 2009. Circumpolar structure and distribution of the Antarctic Circumpolar Current fronts: 2. Variability and relationship to sea surface height. J. Geophys. Res. Ocean 114. https://doi.org/10.1029/2008JC005108.
Stephens, B.B., Keeling, R.F., 2000. The influence of Antarctic sea ice on glacial-interglacial CO_2 variations. Nature 404, 171–174. https://doi.org/10.1038/35004556.
Studer, A.S., Sigman, D.M., Martínez-García, A., Benz, V., Winckler, G., Kuhn, G., Esper, O., Lamy, F., Jaccard, S.L., Wacker, L., Oleynik, S., Gersonde, R., Haug, G.H., 2015. Antarctic Zone nutrient conditions during the last two glacial cycles. Paleoceanography 30, 845–862. https://doi.org/10.1002/2014PA002745.
Sun, X., Matsumoto, K., 2010. Effects of sea ice on atmospheric pCO_2: a revised view and implications for glacial and future climates. J. Geophys. Res. 115, 1–8. https://doi.org/10.1029/2009JG001023.
Svendsen, J.I., Alexanderson, H., Astakhov, V.I., Demidov, I., Dowdeswell, J.A., Funder, S., Gataullin, V., Henriksen, M., Hjort, C., Houmark-Nielsen, M., Hubberten, H.W., Ingólfsson, Ó., Jakobsson, M., Kjær, K.H., Larsen, E., Lokrantz, H., Lunkka, J.P., Lyså, A., Mangerud, J., Matiouchkov, A., Murray, A., Möller, P., Niessen, F., Nikolskaya, O., Polyak, L., Saarnisto, M., Siegert, C., Siegert, M.J., Spielhagen, R.F., Stein, R., 2004. Late Quaternary ice sheet history of northern Eurasia. Quat. Sci. Rev. 23, 1229–1271. https://doi.org/10.1016/j.quascirev.2003.12.008.
Takahashi, T., Sutherland, S.C., Sweeney, C., Poisson, A., Metzl, N., Tilbrook, B., Bates, N., Wanninkhof, R., Feely, R.A., Sabine, C., Olafssong, J., Nojirih, Y., 2002. Global sea-air CO_2 flux based on climatological surface ocean pCO_2, and seasonal biological and temperature effects. Deep Sea Res. 49, 1601–1622. https://doi.org/10.1016/S0967-0645(02)00003-6.
Talley, L.D., 2013. Closure of the global overturning circulation through the Indian, Pacific, and southern oceans: schematics and transports. Oceanography 26, 80–97. https://doi.org/10.5670/oceanog.2013.07.
Tesi, T., Muschitiello, F., Smittenberg, R.H., Jakobsson, M., Vonk, J.E., Hill, P., Andersson, A., Kirchner, N., Noormets, R., Dudarev, O., Semiletov, I., Gustafsson, Ö., 2016. Massive remobilization of permafrost carbon during post-glacial warming. Nat. Commun. 7 (13653) https://doi.org/10.1038/ncomms13653.
Toggweiler, J.R., Russell, J.L., Carson, S.R., 2006. Midlatitude westerlies, atmospheric CO_2, and climate change during the ice ages. Paleoceanography 21 (2005). https://doi.org/10.1029/2005PA001154.
Tribovillard, N., Algeo, T.J., Lyons, T., Riboulleau, A., 2006. Trace metals as paleoredox and paleoproductivity proxies: an update. Chem. Geol. 232, 12–32. https://doi.org/10.1016/j.chemgeo.2006.02.012.
Umling, N.E., Thunell, R.C., 2017. Synchronous deglacial thermocline and deep-water ventilation in the eastern equatorial Pacific. Nat. Commun. 8 (14203), 1–10. https://doi.org/10.1038/ncomms14203.
Vázquez Riveiros, N., Waelbroeck, C., Skinner, L.C., Roche, D.M., Duplessy, J.C., Michel, E., 2010. Response of South Atlantic deep waters to deglacial warming during Terminations V and I. Earth Planet. Sci. Lett. 298, 323–333. https://doi.org/10.1016/j.epsl.2010.08.003.
Veres, D., Bazin, L., Landais, A., Kele, H.T.M., Lemieux-Dudon, B., Parrenin, F., Martinerie, P., Blayo, E., Blunier, T., Capron, E., Chappellaz, J., Rasmussen, S.O., Severi, M., Svensson, A., Vinther, B.M., Wolff, E., 2013. The Antarctic ice core chronology (AICC2012): an optimized multi-parameter and multi-site dating approach for the last 120 thousand years. Clim. Past 9, 1733–1748. https://doi.org/10.5194/cpd-8-6011-2012.
Vogel, H., Meyer-Jacob, C., Thöle, L., Lippold, J., Jaccard, S.L., 2016. Quantification of biogenic silica by means of Fourier transform infrared spectroscopy (FTIRS) in marine sediments. Limnol. Oceanogr. Methods 14, 828–838. https://doi.org/10.1002/lom3.10129.
Volk, T., Hoffert, M.I., 1985. Ocean Carbon Pumps: Analysis of relative strengths and efficiencies in ocean-driven atmospheric CO_2 changes. In: Sundquist, E.T., Broecker, W.S. (Eds.), The Carbon Cycle and Atmospheric CO_2: Natural Variations Archean to Present, Geophysical Monograph Series. American Geophysical Union, Washington, DC, USA, pp. 99–110. https://doi.org/10.1029/GM032p0099.
Völker, C., Köhler, P., 2013. Responses of ocean circulation and carbon cycle to changes in the position of the Southern Hemisphere westerlies at Last Glacial Maximum. Paleoceanography 28, 726–739. https://doi.org/10.1002/2013PA002556.
Watson, A.J., Naveira Garabato, A.C., 2006. The role of Southern Ocean mixing and upwelling in glacial-interglacial atmospheric CO_2 change. Tellus B 58, 73–87. https://doi.org/10.1111/j.1600-0889.2005.00167.x.
Watson, A.J., Vallis, G.K., Nikurashin, M., 2015. Southern Ocean buoyancy forcing of ocean ventilation and glacial atmospheric CO_2. Nat. Geosci. 8, 861–864. https://doi.org/10.1038/ngeo2538.
Yu, J., Elderfield, H., 2007. Benthic foraminiferal B/Ca ratios reflect deep water carbonate saturation state. Earth Planet. Sci. Lett. 258, 73–86. https://doi.org/10.1016/j.epsl.2007.03.025.
Yu, J., Elderfield, H., Jin, Z., Booth, L., 2008. A strong temperature effect on U/Ca in planktonic foraminiferal carbonates. Geochim. Cosmochim. Acta 72, 4988–5000. https://doi.org/10.1016/j.gca.2008.07.011.
Zech, R., 2012. A permafrost glacial hypothesis – permafrost carbon might help explaining the Pleistocene ice ages. Quat. Sci. J 61, 84–92. https://doi.org/10.3285/eg.61.1.07.
Zheng, Y., Anderson, R.F., van Geen, A., Fleisher, M.Q., 2002. Remobilization of authigenic uranium in marine sediments by bioturbation. Geochem. Cosmochim. Acta 66, 1759–1772. https://doi.org/10.1016/S0016-7037(01)00886-9.
Ziegler, M., Diz, P., Hall, I.R., Zahn, R., 2013. Millennial-scale changes in atmospheric CO_2 levels linked to the Southern Ocean carbon isotope gradient and dust flux. Nat. Geosci. 6, 457–461. https://doi.org/10.1038/ngeo1782.

Please cite this article as: Gottschalk, J et al., Southern Ocean link between changes in atmospheric CO_2 levels and northern-hemisphere climate anomalies during the last two glacial periods, Quaternary Science Reviews, https://doi.org/10.1016/j.quascirev.2019.106067